UNIVERSITY OF MODENA AND REGGIO EMILIA

Research Thesis in Science and Technologies for Health Products
(Doctorate School in Science and Technologies for Health Products)

XXV Cicle - PhD Thesis

IN VITRO TOXICITY OF METAL NANOPARTICLES IN NEURONAL CELLS

Thesis of:
Gian Luca Sighinolfi

Tutor:
Prof. Fabio Tascedda

Co-tutor:
Prof. Lorenzo Corsi

Doctorate school coordinator: Prof. Annalisa Tait

Doctorate school director: Prof. Annalisa Tait

INDEX

1.1 INTRODUCTION

Until the last decade, little attention was given by the neuroscience community to the neurometabolism of metals. However, the neurobiology of heavy metals is now receiving growing interest, since it has been linked to major neurodegenerative diseases. As trace elements, heavy metals (e.g. copper, selenium, zinc) are essential to keep the body's metabolism and to preserve the brain function. On the other side, heavy metals might exert negative effects on our body biology due to their bioaccumulation phenomenon. Bioaccumulation means an increase in the concentration of a chemical in a biological organism over time, compared to the concentration of the chemical in the environment. Compounds accumulate in living organisms whenever they are assimilated and stored faster than they metabolized or expelled. Some evidence on the contribution of metals in neurodegeneration came from postmortem studies on patients where it was found an accumulation of these elements in the brain areas of neuronal death. The metals produce dose dependent neurodegenerative damage accounting of several mechanisms: production of free radicals, protein aggregation, metabolic disorders, altered calcium homeostasis and transport of other metals. There are a remarkable variety of pathways activated in several neurodegenerative diseases by particulate material of exogenous origin [1].

1.2 NANOPARTICLES AND NANOTECHNOLOGY

By definition nanoparticles (NPs) are particles with size between 1 and 100 nm [2-3]. They exist in the form of powders and colloidal dispersions. Nanotechnology can be defined as the design, synthesis, and application of materials and devices whose size and shape have been engineered at the nanoscaled range. It exploits unique chemical, physical, electrical, and mechanical properties that emerge when matter is structured at the nanoscaled level. In the assessment of the effects of NPs on human health and biological environment are of great importance the following factors:

- SIZE

  The size of the NPs is different depending on the origin, composition and status of the material. By varying the size of NPs, depending on the composition, is possible to change properties such as solubility, transparency, colour, wavelength of emission or absorption, conductivity, melting point and catalytic behaviour.

  The size also influences the ability of the NPs to diffuse in their solvent [4]. Suspended aerosol NPs are transported by diffusion at a rate inversely proportional to size, they are also subject to Brownian motion (random movements of particles in liquid or gas), tending to collide to form agglomeration. Mobility is inversely proportional to the diameter [5] of the NPs and speed depends on their concentration and mobility in the medium.

- AGGREGATION

  NPs can be held together by strong molecular bonds or weak interactions of Van der Waals forces. Both types of aggregates can be homogeneous, if made from the same type of primary particles, or heterogeneous, consisting of various types of primary particles [6].

The NPs aggregation can be diminished or neutralized using specifical coatings (chemical compounds, binding peptides and other molecules at the surface).

- MORPHOLOGY

  NPs are distinguished by morphology (Fig. 1):

  - Rod NPs types as the nanotubes or nanowires (zig-zag, Helix, tape);
  - NPs not with an elongated shape (spherical, oval, NPs cubic, pyramidal, coil).

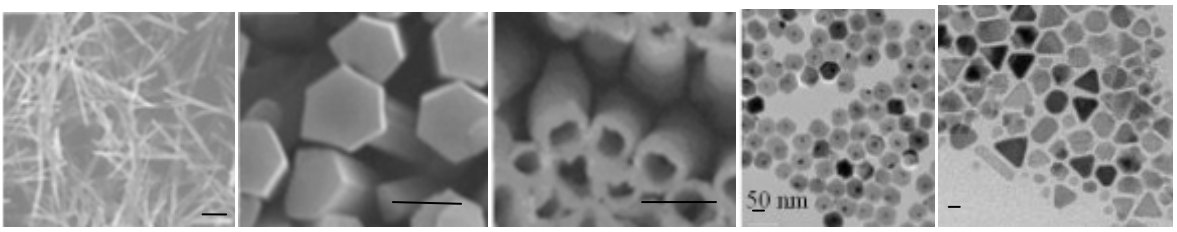

Fig. 1 Typical electron microscopy images of different types of shaped nanoparticles. From left to right: nanowires, nanorods, nanotubes, hexagonally shaped NPs, triangular NPs.

- COMPOSITION

  It consists of a single material or from different materials. NPs in nature usually occur as aggregates of different materials composition, although most of the synthesized NPs are made of single material. Different chemical compositions result in different physical and chemical behaviour.

1.3 SOURCES AND CLASSIFICATION OF NANOPARTICLES

Sources of NPs can be classified as natural or deriving from intentional and unintentional anthropogenic activities. Natural NPs exist in the environment since the beginning of Earth's history and are common and widely distributed throughout the Earths´ atmosphere, oceans, surface and ground water, soil and even in living organisms. Major natural processes that release NPs in the atmosphere are forest fires, volcanic activities, weathering, formation from clay minerals, soil erosion by wind and water, or dust storms from desert [7-8]. Atmospheric dust alone is estimated to contain as much as several million of tons of natural NPs within a year. Naturally occurring ambient NPs are quite heterogeneous in size and can be transported over thousands of kilometers and remain suspended in the air for several days [9].

Man-made NPs are unknowingly or purposely released in the environment during various industrial and mechanical processes. These NPs are very heterogeneous in nature and currently it is difficult to measure the impact on human health. The annual release of human produced NPs into the environment cannot be accurately estimated while production volumes are strongly increasing. The unfiltered exhaust gases from diesel engines contain large quantities of potentially harmful NPs from the incomplete combustion of fuel [10]. In the fireplace at home, fullerenes like buckyballs or buckytubes are formed when wood is burned. In industrial processes, coal, oil, and gas boilers release tons of NPs unintentionally [11-13].

As a growing and widely applied science, nanotechnology has a global socioeconomic value, with applications ranging from electronics to biomedical uses.

Because of their small size (less than 100 nm) and the very high surface to volume ratio, NPs usually display an enormously elevated reactivity potential. NPs can be assigned to a transitional range between single atoms or molecules and bulk material. The physicochemical features of NPs differ substantially from those of their respective bulk materials. Most of the anthropogenic NPs are made up of carbon, silicon, metal or metal oxides and are believed to adversely affect the environment and human health directly or indirectly together with naturally occurring NPs [14]. A commonly used classification divides nanomaterials products from nanotechnology, based on the nature and the specific features of NPs:

- Carbon nanomaterials: primarily carbon compounds. According to their shapes can be divided into fullerenes, carbon nanotubes, NPs, nanofibers. These materials, thanks to their extraordinary physical and chemical properties (light weight, strength, chemical and thermal stability, conductivity) are interesting for various applications: they are used in biomedical devices or fluorescent contrast agents but may also be used in drug delivery [15].
- Semiconductor nanomaterials: better known as quantum dots, are highly packaged semiconductor crystals of hundreds or thousands of atoms. These materials are used in cellular imaging, exploiting their ability to emit fluorescence. The electron density and composition of these materials made it possible to exploit them as probes in conventional electron microscopy and drug delivery [16-17].
- Metal nanomaterials: metal compounds are characterized by a metallic material in nanometer scale and include, gold, cobalt, SPIO (Super Paramagnetic Iron Oxide) and other metal oxides such as cerium oxide (CeO_2) NPs. These materials are now the most studied and found important applications in drug delivery, gene delivery, diagnostic and basic research [18].

A further important classification can be made depending on the coating, according to these criteria, the NPs are divided into "naked" (uncoated) and "coated" (covered). The presence or absence of coating (polyethylene glycol, agarose, dextran, copolymers and lipids etc) interferes with the ability of nanoparticle to interact with its target [19-20].

The coating assume pharmaceutical importance as it could direct modify NPs affinity and to drive NPs to specific targets, improving the ligand-receptor interaction and lowering toxicity. Promising results have been reported in the diagnosis and treatment of cancer using lipid-coated NPs. These nanostructures can load both hydrophilic drugs in the small hydrophilic cores. Lipid coating also facilitates the absorption of the drug through biological membranes and interaction with negatively charged nucleic acids [21].

1.4 NANOPARTICLES PORTALS OF ENTRY AND TARGET TISSUES

Nanoparticles, due to their small size, high reactivity and high surface area, can penetrate the human body in several ways: by ingestion (gastrointestinal tract), inhalation (respiratory tract), dermal (skin) and injection (bloodstream) (Fig.2) [22].

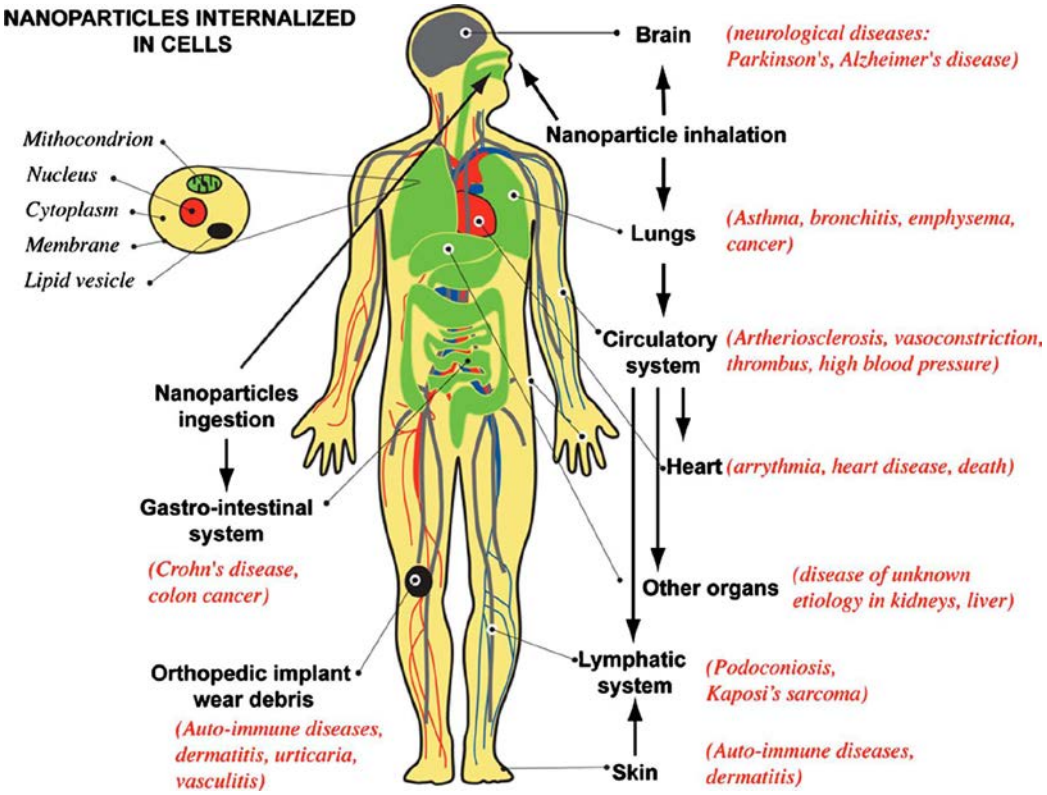

Fig. 2 Schematics of human body with pathways of exposure to NPs, affected organs, and associated diseases from epidemiological *in vivo* and *in vitro* studies.

1.4.1 INGESTION

Exogenous sources are particles from food (such as colorants, e.g., titanium oxide), pharmaceuticals, water, cosmetics (toothpaste and lipstick), dental prosthesis debris and inhaled particles.

The extent of particle absorption in the gastrointestinal tract is affected by size, surface chemistry and charge, time and dose exposure [23].

The exact order of translocation from the gastrointestinal tract to organs and the blood is not known; however, a case study of dental prosthesis porcelain debris internalized by intestinal absorption suggests that intestinal absorption of particles is followed by liver clearance before they reach the general circulation and the kidneys [24]. NPs have been found consistently in colon tissue of subjects affected by cancer, Crohn's disease, and ulcerative colitis, while in healthy subjects, NPs were absent [25]. The NPs present in these patients had various chemical compositions and are not considered toxic in bulk form. Microscopic and energy-dispersive spectroscopy analysis of colon mucosa indicated the presence of carbon, ceramic silicates, gypsum, sulphur, calcium, silicon, stainless steel, silver and zirconium. The size of debris varied from 50 nm to 100 µm, the smaller the particle the greater the degree to penetrate. The particles were found at the

interface between healthy and cancerous tissue. Based on these findings, it was suggested that the gastrointestinal barrier is not efficient for particles smaller than 20 µm.

1.4.2 INHALATION

Due to its large surface area, the lung is another primary route of entry for inhaled particles [26-29]. The first contact of inhaled NPs in the respiratory tract is with the lining fluid, composed of phospholipids and proteins. This contact leads to particle wetting and to their spreading towards the epithelium by surface forces from the liquid-air interface. PM10 (particles with a diameter less than or equal to 10 µm) are inhalable dust, that is able to penetrate and settle in the upper respiratory tract (nose, pharynx and larynx) and are eliminated by mucociliary action. The PM 2.5 (particles with a diameter less than or equal to 2.5 µm) are inhalable dust which can penetrate into the lower respiratory tract (from trachea to pulmonary alveoli). NPs (ultrafine particles, UFP) with small sizes (<100nm), are able to reach and exceed the alveoli and mucous membranes. These NPs are phagocytized by alveolar macrophages infiltrating the interstitial space and entering the circulatory and lymphatic system until they settle in various internal organs such as liver, kidney and intestine.

1.4.3 DERMAL CONTACT

Recent studies on vaccines have assessed the entrance of NPs through skin and it has been shown that only small particles (40 nm), are able to diffuse through the skin barrier as opposed to larger particles (750 nm and 1500 nm). Once reached the dermis, the particles are able to penetrate into capillaries and to flow into the systemic circulation. In this regard it is important to mention that titanium dioxide NPs are capable to reach the circulatory stream crossing the skin barrier in a few minutes [30-32].

1.4.4 LYMPHATIC SYSTEM

Translocation of NPs to lymph nodes is a topic of intense investigation today for drug delivery and tumor imaging. The progression phase of many cancers (lung, esophageal, mesothelioma, etc.) account of the spread of tumor cells to local lymph nodes. Several studies show that interstitially injected particles pass preferentially through the lymphatic system and not through the circulatory system, probably due to permeability differences. After entering the lymphatic system, they locate in the lymph nodes. The free NPs reaching the lymph nodes are ingested by resident macrophages.

NPs that are able to enter the circulatory system can also gain access to the interstitium and from there are drained through the lymphatic system to the lymph nodes as free NPs and/or inside macrophages [33-34].

1.4.5 CIRCULATORY SYSTEM

Inhalation or instillation studies in healthy animals show that metallic NPs with size smaller than 30 nm pass rapidly into the circulatory system while non-metallic NPs with size between 4 and 200 nm pass very little or not at all. In contrast, subjects suffering from respiratory and circulatory diseases have higher capillary

permeability, allowing fast translocation of metallic or non-metallic NPs into circulation. From the circulatory system, long-term translocation to organs (such as the liver, heart, spleen, bladder, kidney, and bone marrow) is possible, depending on the duration of exposure. Smaller particles (20 nm) are cleared faster from the lungs than larger particles (100 nm), probably because small NPs are not efficiently phagocytized by macrophages and are able to enter more rapid the circulatory and/or lymphatic systems [35-38].

Several epidemiological studies have shown that increased concentrations of particulate air pollution are linked to increased cardiovascular mortality, mortality from arteriosclerosis, myocardial ischemia and infarction in the short term. Contact with environmental ultrafine particles triggers an inflammatory response and this may be an important factor leading to the cardiovascular damage (Fig. 2) [39].

1.5 TOXICOLOGICAL PROPERTIES OF NANOPARTICLES

In the past decade, toxicological studies have demonstrated that small NPs (<100 nm) cause significant toxicity and adverse respiratory health effects [40-41]. Generally, the negative health effects of NPs do not correlate with NPs mass dose. This led to the conclusion that the surface area of NPs plays a crucial role in their potential toxicity. Indeed, smaller NPs have an higher surface area and particle number per unit mass compared to larger particles. In vitro experiments demonstrated that larger surface area leads to increased reactivity and is an increased source of reactive oxygen species. Furthermore the higher surface area of NPs produces a dose-dependent increase in oxidation and DNA damage, much higher than larger particles with the same mass dose [42-43].

There are many contradictory results related to the toxic effects of NPs at different concentrations. Some studies show that certain materials are not as toxic as was observed by other studies. When comparing the results of different studies, it must be taken into account that there are differences in the aggregation properties of NPs in air and water, resulting in inherent discrepancies between inhalation studies and instillation or in vitro experiments. The aggregation may depend on surface charge, material type, and size, among others [44].

Cellular uptake, subcellular localization, the ability to catalyze oxidative products and organelle injury seem to be directly related to nanoparticle chemistry, size, and shape [45-46].

The mechanism by which NPs penetrate cells is supposed to be initiated by Van der Waals - electrostatic - steric forces or interfacial tension effects. This type of passive uptake without a phagosome formation and the hypostatized free movement of NPs within the cell, concerns about their ability to have direct access to cytoplasm proteins and organelles. On the other side, NPs may also be internalized by professional phagocytes such as alveolar macrophages and various types of cells, including endothelial cells, pulmonary epithelium, gastrointestinal epithelium, red blood cells, platelets, and neuronal microglia cells.

While the precise mechanism whereby NPs induce pro-inflammatory effects is not known and due to these evidences and according to previous studies, it has been suggested that NPs create reactive oxygen species (ROS), and thereby modulate intracellular calcium concentrations, activate transcription factors, and induce

cytokine production [47-49]. On the contrary some i*n vitro* and *in vivo* experiments demonstrate that exposure to some NPs can produce cell death via mitochondrial damage without inflammation [42]. The figure 3 displays a very simplified and schematic interpretation of the current understanding of these very complex cellular mechanisms.

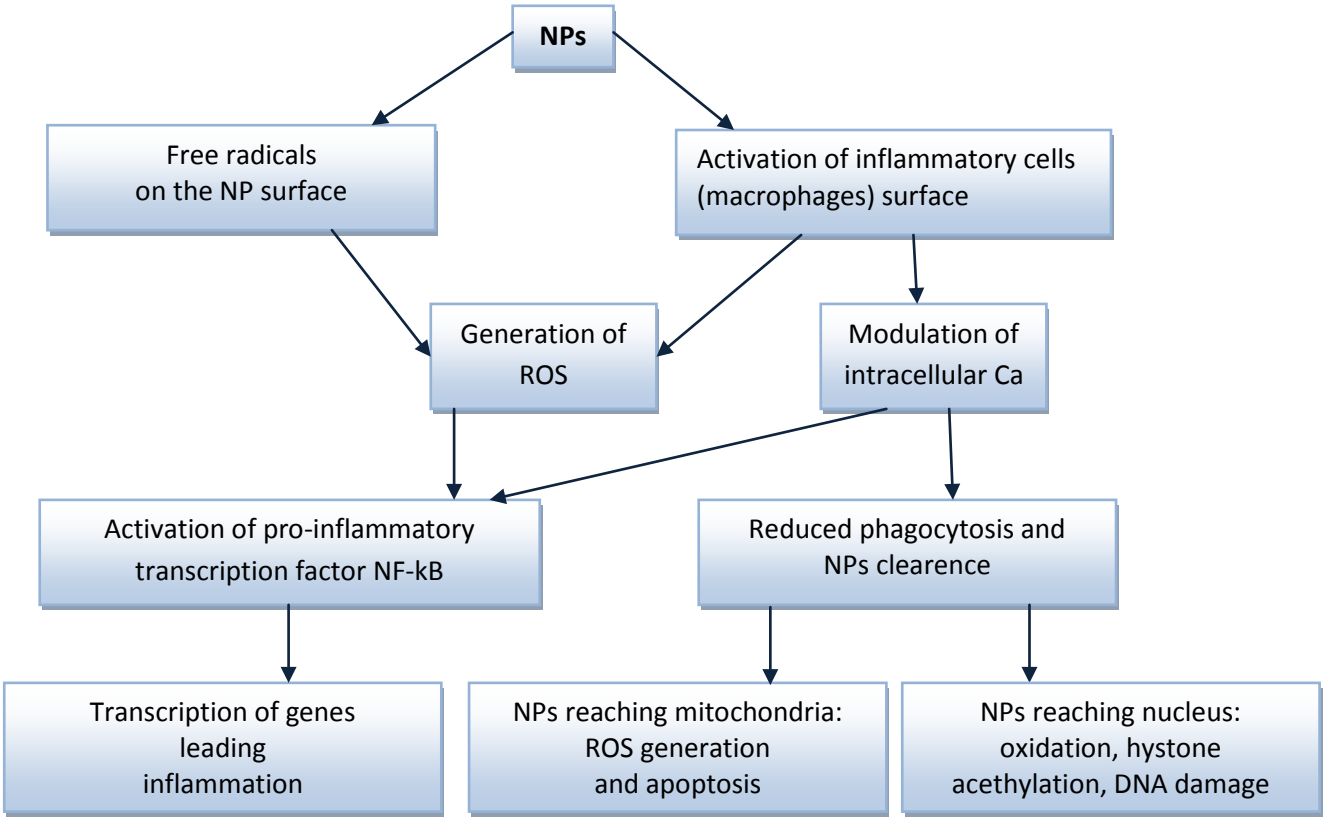

Fig. 3 Schematics of the molecular events by which NPs exert their toxic effects at the cellular level.

1.6 NANOPARTICLES AND THE CENTRAL NERVOUS SYSTEM

Experimental evidence suggests that the initiation and promotion of neurodegenerative diseases, such as Alzheimer's disease, Parkinson's disease, and Pick's disease, are associated with oxidative stress and with the presence in the brain of protein material that is not readily removed by proteolytic enzymes [50-53]. In addition to protein material there are other particles, of exogenous origin, which can settle into the brain and accumulate. These particles may promote oxidative stress and brain inflammation in the same manner as aggregates of endogenous origin described above: among these compounds NPs are to be taken in consideration [54]. Some examples of such diseases are given in Table 1.

Neurodegenerative disorder	Accumulating particles	Protein associated with insoluble material
Alzheimer's disease	Amyloid plaques, neurofibrillary tangles	β-amyloid peptides, Hyperphosphoylated tau
Dementia with Lewy Bodies (DLB)	Lewy bodies	
Parkinson's disease	Lewy bodies	α-synuclein
Huntington's disease	Intranuclear inclusions	Huntingtin protein with expanded glutamine repeats
Spinocerebellar ataxia type 3	Intranuclear inclusion	Ataxin-3 with expanded glutamine repeats
Down's syndrome	Lewy bodies, amyloid plaques	α-synuclein, β-amyloid
Human variant of Bovine spongy encephalopathy, Creutzfeldt-Jakob disease	Amyloid plaques	Prion protein variant
Pick's disease	Pick bodies	Hyperphosphorylated tau

Table 1. Protein and particle inclusions associated with specific neurological diseases.

Recent studies have shown how the UFP airborne are able to pass directly through the nasal mucosa and reach the brain for transport trans-synaptic, then the bulb and olfactory nerve are excellent route of entry towards the central nervous system to the NPs (especially under high environmental and occupational exposure of NPs, but also under chronic exposure) [55-57]. Figure 4 illustrates the ways through which NPs can move to the brain following inhalation.

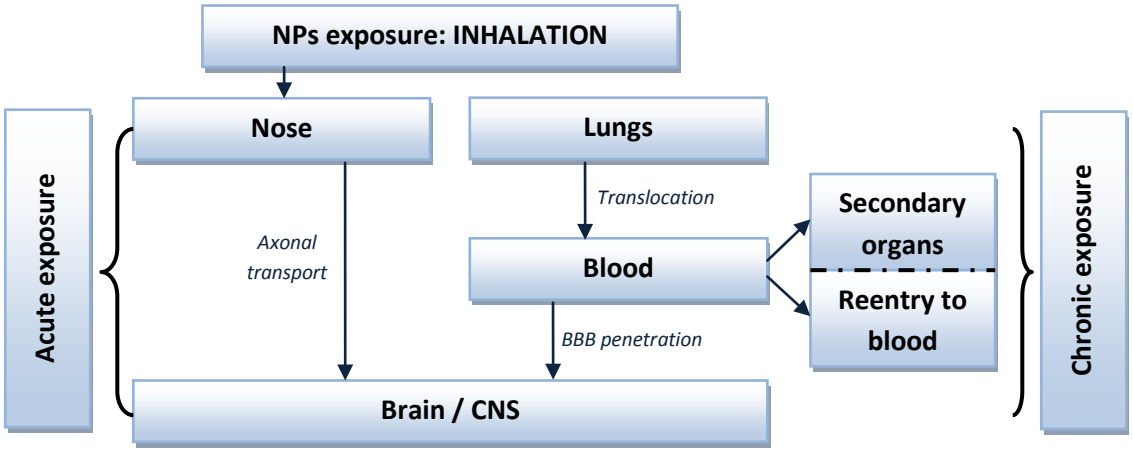

Fig. 4 Routes through which the inhaled NPs can move to the brain.

It was seen that instilling gold NPs of 50 nm in monkey's nose, these NPs moved through the axons of olfactory nerves to the olfactory bulbs and locating selectively in the mitochondria and not in the cytoplasm [22]. Nanomaterials that circulate in the blood can enter the central nervous system (CNS) through the blood–brain barrier (BBB). The blood-brain barrier consists of endothelial cells of brain capillaries held together by tight junctions protecting the central nervous system from xenobiotics and endogenous potentially damaging molecules. Since the tight junctions of the BBB have a gap of only 4-6nm it is thought that the NPs pass

through the membrane of endothelial cells rather than through the junctions between cells. It is also known that in many diseases, like hypertension or allergic encephalomyelitis the BBB permeability is reduced and small NPs (<50nm) can pass the barrier [57,59].

Nanoparticle surface charge can also alter the integrity of the blood-brain barrier, with possible consequences on the use of nanomaterials for drug delivery in CNS, and also in brain toxicity[60]. Of the two major cell types of the nervous system (neurons and glial cells), neurons have characteristics that make them particularly sensitive to different types of stressors. Neurons have an anatomy particularly vulnerable due to their very thin and fragile extensions (dendrites and axons especially). In addition these cells are metabolically very sensitive. Certain types of metal NPs have been already identified as promoters and enhancers of neuronal inflammation: titanium NPs enhance normal brain response to inflammatory agents such as lipopolysaccharide and activate the microglia; in a similar way also act silver NPs, iron oxide and manganese oxide [61-65].

The mechanism by which NPs and colloids relatively inert form a hotbed of inflammation may involve their high surface area, their coating and their electrostatic interactions. By surface charge, NPs can attract metal ions, proteins or other particles and produce reactive oxygen species and a subsequent prolonged inflammatory reaction. The importance of metal-particle interaction is evident in the case of asbestos particles which are able to attract and bind onto the surface iron ions and cause oxidative damage to DNA. This activity, can be suppressed by Desferal, a powerful iron chelator [66]. Iron oxide NPs (Fe_3O_4 NPs) have been recently found cytotoxic on rat pheochromocytoma PC12 cells line [67].

The results showed that exposure to Fe_3O_4 NPs decreased cell viability respectively in a dose dependent manner. Also copper oxide NPs have shown to be cytotoxic and genotoxic in mouse Neuro-2A neuroblastoma cell line [68].

Even on glial cells the NPs exhibit a toxic effect. This it could be logic if we consider that glial cells might act also as scavenger of different metabolites/compound and it is the immune system of the central nervous system (CNS).

Microglia comprise 12% of the cell population of the CNS and are macrophage-like cells resident within the CNS [69]. Microglia are regarded as important mediators of the initial inflammation in the CNS. Abundant experimental evidences have demonstrated that inflammation mediated by microglia contributes to neurodegenerative diseases, including Parkinson's disease and Alzheimer's disease [70-72]. Upon activation, microglia are capable of releasing various molecules, such as nitric oxide (NO), reactive oxygen species (ROS), TNF-±, IL-1± and IL-6, that play important roles in neuronal injury and apoptosis [73].

To date, *in vitro* studies regarding the inflammation caused by NP-stimulated-microglia have primarily focused on the mechanism of ROS-mediated oxidative stress [74-75].

Recently, other pro-inflammatory factors produced by microglia have been gaining increased attention. Wang et al. (2011) reported that BV-2 microglial cells exposed to Fe_2O_3 NPs generated not only ROS but also NO. Choi et al. (2010) reported that silica NPs(ranging from 150 to 200 nm in diameter) increased the

production of intracellular ROS/reactive nitrogen species (RNS) and induced the expression of TNF-±, IL-1± and cyclooxygenase-2 in microglial cells [76-77].

In summary, the potentially toxic effects of various inorganic NPs on neuronal function remain largely unknown ,especially for those NPs of diameters less than 100 nm.

2. AIM OF THE THESIS

Currently there are only few studies on the interaction between NPs and the central nervous system and in particular their possible toxic effect at neuronal and glial cell level. The present study investigated the role of insoluble metal NPs on several cell types including microglia and rat primary cortical cells to detect their possible impact on neurodegeneration and related mechanisms.

Objectives of this work were the identification of the potential effects of NPs evaluating in-vitro cell proliferation and viability according to standard ISO/EN 10993-5 tests of cytotoxicity.

Furthermore an innovative aspect of the study focused to identify the cancerogenic potential of NPs using a never before applied test which mimics the in vivo onset of carcinogenicity.

This new strategy for toxicological and cancerogenic tests could provide important results on the real potential toxicity of NPs to the neuronal cells.

2.1 TESTED METAL NANOPARTICLES

Gold (Au), iron oxide (Fe_3O_4), cobalt (Co) and cerium oxide (CeO_2) metal NPs were selected and tested. NPs of gold and iron oxide were chosen for their recent use in magnetic resonance imaging, cancer therapy and drug delivery. Cerium oxide NPs were selected for their significant presence as air pollutants released by catalytic converters; ultimately cobalt NPs were chosen for their marked physical and chemical toxicity.

Here is a brief summary of selected NPs main uses:

• GOLD

Gold as a colloid had many early applications in medicine: it was used for the treatment of tuberculosis, syphilis and rheumatoid arthritis. It was considered helpful against Alzheimer's disease and also in the therapy of pain and bronchial asthma [78-79].

Gold NPs applications in the biological field are currently arising. Gold NPs are in studio as carriers of drugs, in the treatment of cancer (Photothermal cancer therapy) and as contrast medium for advanced imaging methods (AFM, MRI).

• IRON OXIDE

Iron oxide NPs are used in medicine as a contrast agent for magnetic resonance imaging due to their strong paramagnetic properties (SPIO). These NPs are currently being investigated for the treatment of cancer cells (cancer hyperthermia treatment) and for drug delivery (delivery of specific drugs). Iron oxide NPs have a long retention time in blood and are generally considered safe although toxicity data are still ambiguous [80-83].

• COBALT

Cobalt NPs were tested as their toxicity was already described in the literature: the particles are quickly captured by the cells and remain confined to vesicles in the cytoplasm and induce a rapid increase of ROS.

Even Ponti et al. have conducted studies of cytotoxicity, genotoxicity and morphological transformation on NPs of cobalt and cobalt ions in Balb/3T3 cells. They found that cobalt NPs are genotoxic causing the *in vitro* formation of type III foci.

Later studies in rabbits and rodents showed that NPs and cobalt ions are genotoxic *in vivo*. Occupational exposure to cobalt dust is linked to an increased risk of lung cancer, probably due to the production of ROS, and the inhibition of DNA repair mechanisms [84-87].

• CERIUM OXIDE

Cerium oxide (CeO_2) NPs are used as a polishing agent embedded in the walls of self-cleaning ovens and as a catalyst in the vehicle industry. Cerium oxide is a powerful oxidizing agent and is able to react with combustible organic materials at high temperatures. Workers exposed to cerium have experienced itching, sensitivity to heat and skin lesions; animals injected with large doses of cerium oxide have died from cardiovascular collapse [88-89]. No literature data was found on NPs possible neurotoxicity.

3. MATERIALS AND METHODS

3.1 CELL CULTURES

3.1.1 IMMORTALIZED CELL CULTURES

Two human neural culture cell lines, SH-SY5Y and U-87, were used as models of neurons and astrocytes respectively. The SH-SY5Y human neuroblastoma cell line exhibited typical epithelial morphology. These cells propagated by mitosis and expanded by extending neurites in the surrounding areas. SH-SY5Y cells formed clusters related to their cancerous nature. The U-87 glioblastoma cell line showed epithelial-like morphology (Fig. 5).

The murine BV-2 cell line was used as a model of microglia. The BV-2 cells have morphological, phenotypical and functional markers of macrophages. The BALB 3T3 cell line, although immortalized in vitro, is reportedly non-tumorigenic and was used to detect a possible transformation induced by the NPs.

The cell lines were provided by Istituto Zooprofilattico Sperimentale della Lombardia e dell'Emilia Romagna ("Bruno Ubertini" cell bank).

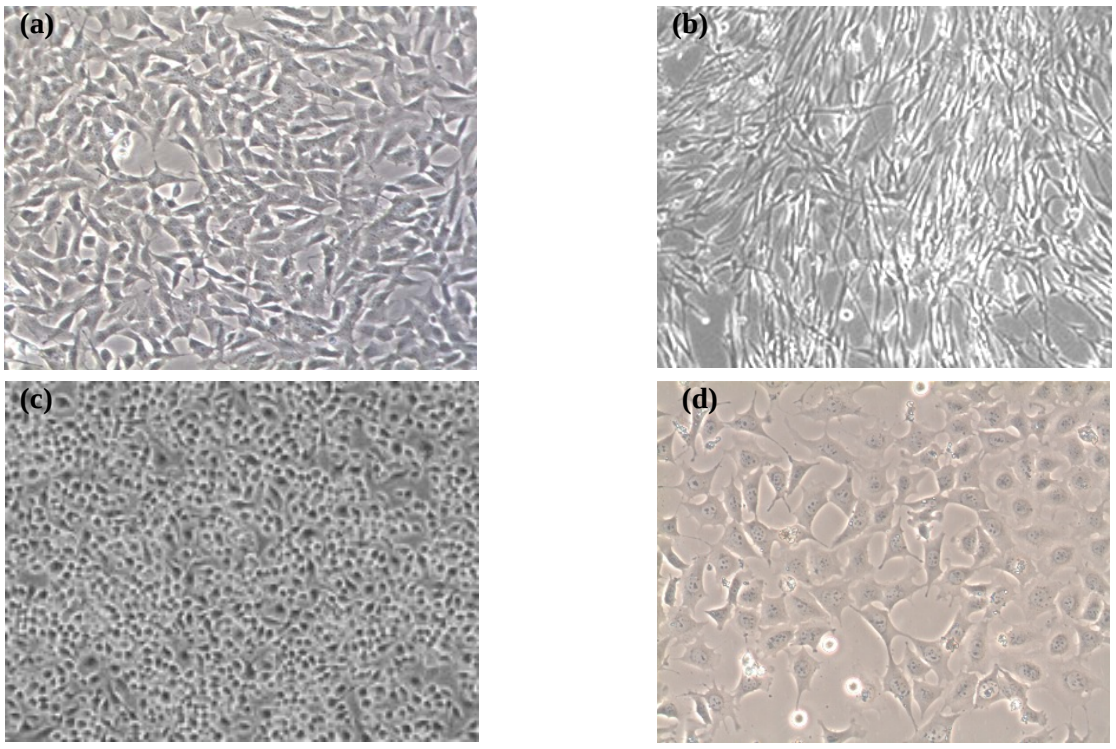

Fig. 5 SH-SY5Y cells (a), U-87 cells (b), BV-2 cells (c), BALB 3T3 cells (d) images by optical microscopy. (10X)

Unlike primary cell cultures, the SH-SY5Y, U-87, BV-2 and BALB 3T3 cell lines are immortalized cell lines that are capable to divide indefinitely. These cells grow in a monolayer and terminate their division when they cover the total surface of the plate, presenting contact inhibition.

The immortalized cell lines have been cultured at 37° C in a humidified atmosphere with 5% of CO_2 in appropriate cell culture medium (3.2).

3.1.2 PRIMARY CELL CULTURES

To simulate the in-vivo brain condition primary cell cultures derived directly from the dissociation of rat cortex tissues were used. Both neural and glial cell sub populations were co-cultured and plated. Primary cultures do not have any proliferative capacity and last only 8-10 days, after which senescence occurs. The cell cultures were maintained in a special growing medium (3.2) at 37° C in a humidified atmosphere with 5% CO_2.

3.2 CELL CULTURE MEDIUM

To culture the SH-SY5Y, U-87, BV-2, BALB 3T3 and the primary neuronal cells, standard Dulbecco's Modified Eagle's Medium (DMEM) growing medium was used.

DMEM was supplemented with the following reagents to obtain 500 ml of final volume:

- 50 ml FBS (Fetal Bovine Serum)
- 10 ml L-Glutammine
- 3 ml Penicilline-Streptomicine
- 6 ml Sodium Piruvate

All the reagents including DMEM were purchased from Invitrogen/Life technologies (UK).

3.3 CELL CULTURE TECHNIQUES

3.3.1 IMMORTALIZED CELL CULTURES TECHNIQUES

The SH-SY5Y, U-87, BV-2 and BALB 3T3 cell lines were cultured under sterile conditions using common guidelines. Cells were cultured as monolayers in growth medium at 37°C in a humidified 5% CO_2 atmosphere. The medium was changed every 3 days. When cells reached 80‑90% confluence, they were washed twice with Phosphate Buffer Saline (PBS) and detached by incubating them with trypsin (0.25%) for 5 min, washed twice with the growth medium, and then resuspended in growth medium at a density of 5×10^4 cells/100 mL flask. Subsequent passages were performed when cells reached confluence. Cell count was performed with 50 µl of cell suspension and 50 µl of trypan blue solution using a Burker chamber. Trypan blue is a dye capable to selectively stain dead cells. Live cells do not allow the stain to penetrate inside the cytoplasm due to their membrane integrity. This method allows to detect and count by optical microscopy only viable cells. The above procedure was repeated every three days for the duration of the experiment to enable the maintenance of cell lines. All reagents including PBS were provided by Invitrogen/Life technologies (UK).

3.3.2 PRIMARY RAT NEURONAL CELL CULTURES TECHNIQUES

The primary rat cortex neurons and glial cells were isolated from micro-surgically dissected regions of Sprague/Dawley rats (Sprague River Laboratories Italy). These cells were prepared freshly using day one neonatal rats and dissection/dissociation technique. The following solutions were prepared before the procedure and then used:

SOLUTION 1: 15 ml KREB 10x in 135 ml of H_2O

450 mg of BSA and 1.6 ml of $MgSO_4$ (pH 7.4).

SOLUTION 2: 25 ml of solution 1 with 6.25 mg of trypsin.

SOLUTION 3: 15 ml of solution 1 with 1.6 mg of DNAse.

7.75 mg of trypsin inhibitor and 150 µl of $MgSO_4$

SOLUTION 4: 4 ml of solution 3 with 21 ml of solution 1.

SOLUTION 5: 12.5 ml of solution 1 with 15 µl of $CaCl_2$ and 100 µl of $MgSO_4$

Once prepared the solutions the following protocol was applied:

- the cortices were dissected, meninges were removed and the dissociated tissue was transferred to a 50 ml tube containing the previously prepared solution 1. The sample was centrifugated for 1 minute at 1000 rpm;
- the supernatant was discarded and the solution 2 was added to obtain enzymatic digestion. The sample was kept at 37° C for 13 minutes;
- the solution 4 was added to the dilution few seconds before centrifugation (1 minute at 1000 rpm);
- the supernatant was discarded and 2-3 ml of solution 3 were added. Later the second mechanical dissociation was carried out;
- the solution 5 was added to the dilution and the sample was centrifuged for 5 minutes at 800 rpm;
- the supernatant was removed and the pellet was re-suspended in 10-15 ml of medium;
- 5 µl of the final solution were used to perform cell count;
- finally 800,000 cells were plated in 35 mm diameter petri dishes containing a total amount of 2.5 ml of medium.

After two hours from cell seeding the medium was changed. The cells were maintained under the conditions described in primary cell cultures paragraph.

3.4 NANOPARTICLES CHARACTERIZATION

3.4.1 DRY NANOPARTICLES

Au, Co, Fe_3O_4, CeO_2 NPs in powder form were obtained from Nanostructured & Amorphous Materials Inc. (Houston, USA). Before usage, the NPs were depirogenated for 100 min at 190°C. NPs were then re-suspended in PBS and sonicated using Branson 3510 Ultrasonic bath (Branson Ultrasonics, Danbury USA) for 20 min using the OECD WPMN guidance and program for the testing of Manufacture Nanomaterials. NPs composition data and characteristics are summarized in the following tables (Tab. 2-5).

Table 2. Au NPs (99,5%)

COMPOSITION	**Gold**
SHAPE	Spheric
SIZE (diameter)	35 nm
BULK DENSITY	1,0 g/cm^3
TRUE DENSITY	19,32 g/cm^3
COLOR	yellow

Table 3. Co NPs (99,8%)

COMPOSITION	**Cobalt**
SHAPE	Spheric
SIZE (diameter)	28 nm
BULK DENSITY	0,10-0,25 g/cm^3
TRUE DENSITY	8,92 g/cm^3
COLOR	black

Table 4. Iron Oxide NPs (99,5%)

COMPOSITION	**Iron Oxide (Fe_3O_4)**
SHAPE	Spheric
SIZE (diameter)	15-20 nm
BULK DENSITY	0,8-0,9 g/cm^3
TRUE DENSITY	4,8-5,1 g/cm^3
COLOR	black (not graphite black)

Table 5. Cerium Oxide NPs (99,9%)

COMPOSITION	**Cerium Oxide (CeO_2)**
SHAPE	Spheric
SIZE (diameter)	15-30 nm
BULK DENSITY	< 0,2 g/cm^3
TRUE DENSITY	7,132 g/cm^3
COLOR	pale yellow

NPs suspensions were analyzed to determine size, particle concentration, surface charge and aggregation using the following techniques:

- Dynamic Light Scattering (DLS) - (Malvern Zeta Sizer Nano ZS)
- Zeta Potential Analyzer - (Malvern Zeta Sizer Nano ZS)
- Transmission Electron Microscopy (TEM) – (JEM 2010, Jeol - Oxford Instruments)

3.4.2 DLS NANOPARTICLES ANALYSES

DLS analyzes were performed to obtain information on NPs average diameter and distribution/aggregation state in solution. With DLS technique the sample is illuminated by a laser beam and a detector measures, as a function of time, variations in intensity of the light being scattered. These variations are generated by the Brownian motion of scattered particles on the interacting source. At equal temperature and viscosity, smallest particles move/diffuse more rapidly than larger particles, creating different variations of intensity reported in the basis of Polydispersity Index (PDI), an indicator of the width of the particle size distribution.
The DLS measures the speed of the variations in intensity and calculates the coefficient of diffusion of the particles. Applying the Stokes-Einstein equation, the software automatically converts the diffusion coefficient in the hydrodynamic diameter.

3.4.3 ZETA-POTENTIAL ANALYSES OF NANOPARTICLES

Zeta potential is a critical parameter that predicts colloidal stability, aggregation and dispersion of NPs in a solution. Zeta Potential is a measurement of the surface charge of dispersed NPs and is quantified in mVolt. The principle consists in the detection of electrophoretic mobility of the particles in an electrical field using the Smoluchowski equation considering the electric permittivity of solvent. NPs with Zeta Potential values greater than +25 mV or less than -25 mV have typically high degrees of stability. Dispersions with a low zeta potential value will eventually aggregate due to Van Der Waals inter-particle attractions.
Measuring NPs zeta-potential is therefore critical to understand the electronic, thermal and chemical properties of the NPs. The Zeta Potential of the NPs dispersions was performed following analogue sample preparations used for the DLS analyses utilizing the ZetaSizer Nano ZS (Malvern Instruments Inc, UK).

3.4.4 TRANSMISSION ELECTRON MICROSCOPY (TEM)

Imaging and analytical characterization of NPs to assess NPs dimensions, shape, size and morphology were achieved by Transmission Electron Microscopy (TEM).
Transmission electron microscopy uses a high energy electron beam transmitted through a very thin sample interacting with the specimen which is passed through. The electrons transmitted through the specimen are collected and processed as an image with atomic scale resolution.
TEM mode provides imaging contrast that is a function of the sample thickness and of the sample material: NPs show a higher scattering power than the normal atoms of a protein (C, H, N, O and S) and therefore they

appear brighter. The sample preparation method consisted in placing a small drop of the stock NPs solution on a carbon coated copper grid (2M Strumenti Italy) followed by vacuum drying for 5min.

3.5 CYTOTOXICITY TESTS

Two in vitro colorimetric assays were used to assess the cytoxicity of the different NPs. XTT assay was performed to determine the viability of the cells and BrdU ELISA was used to quantify cell proliferation by the detection of newly synthesized DNA in actively duplicating cells.

3.5.1 XTT VIABILITY ASSAY

The XTT method is a colorimetric assay designed for the spectrophotometric quantification of cell viability. The assay is based on the cleavage of the yellow tetrazolium salt (XTT) to form an orange formazan dye by metabolic active cells. This conversion occurs exclusively in viable cells (Fig. 6). The formazan dye formed is soluble in aqueous solutions and it is directly quantified using a scanning multiwell spectrophotometer at 492nm wavelength. An increase in number of living cells results in an increase in the overall activity of mitochondrial dehydrogenases in the sample. This increase directly correlates to the amount of orange formazan produced, as monitored by the UV light absorbance.

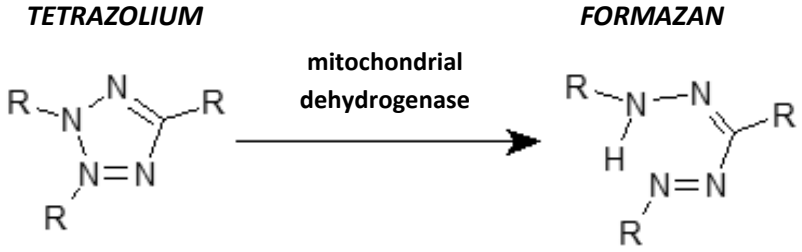

Fig. 6 Principle of XTT assay: tetrazolium conversion in formazan.

Cell viability was evaluated on both immortalized and primary cell lines after 48h and 72h of contact with the NPs. Cultures wells without cells were used as blanks, while cells supplemented with 0.125% (w/v) phenol (Sigma Aldrich, St Louis USA), a cytotoxic agent, were used as a positive control. NPs spectrophotometrical interference was estimated using preliminary readings with NPs solution only, NPs solution and medium, and NPs solution with XTT labeling mixture. Non treated cells were used as negative control.

3.5.2 XTT ASSAY ON IMMORTALIZED CELL LINES

Cells (SH-SY5Y, U-87, BV-2) were plated in 96 wells microplates (NUNC wellplates Micro, USA) at a concentration of $7x10^3$ cells/well in a volume of 100 µl of medium. After 3 hours of incubation the cells were treated using the four types of metal NPs at the following dilutions (Tab. 6):

150.00	µg x 10^6 Cells
15.00	µg x 10^6 Cells
1.50	µg x 10^6 Cells
0.15	µg x 10^6 Cells

Tab. 6 Tested NPs dilutions.

The XTT labeling mixture was readily prepared by mixing 5 ml XTT labeling reagent with 0.1 ml of electron coupling reagent. After 48 or 72h of NPs contact, 50 µl of XTT labeling mixture solution was added to each well. The cells were then incubated at 37° C for 8 hours. After 8 hours the plates were red using a spectrophotometer (Multiskan RC, ThermoLabsystemsTM, Finland) at a wavelength of 492 nm.

3.5.3 XTT ON NEURONAL RAT PRIMARY CELLS

To perform this test, rat primary cells were cultured for three days in 33 mm Petri dishes. After three days the cells were then treated with the NPs at the dilution of 1.5 µg x 10^6/cells.

All the experiments were performed in triplicate using control plates, in which cells have not made contact with the NPs.

After 72h of cell/NPs contact the XTT labeling mixture solution was added to each plate. The cells were then incubated at 37° C for 8-12 hours. Later the reaction medium was collected from each Petri plate and red using a spectrophotometer at a wavelength of 492 nm.

3.5.4 BrdU ELISA CELL PROLIFERATION ASSAY

BrdU cell proliferation assay kit (Roche Applied Science, Mannheim, Germany) was used to measure cell proliferation by quantifying BrdU incorporated into the newly synthesized DNA of S-phase replicating cells. 5-bromo-2'-deoxyuridine (BrdU) is a synthetic thymidine analog that is incorporated into newly synthesized DNA during cell replication of actively proliferating cells.

Each different cell type was cultured in 96-well multi plates (NUNC Micro well plates, USA) at a concentration of $7x10^3$ cells per well in a final volume of 100 µl/well (Fig. 7). The cells were treated with NPs (1.5 µg/10^6 cells) which were directly added to the medium and incubated for 48h and 72h. After incubation, 10 µl/well of BrdU labelling solution (Cell Proliferation ELISA, BrdU, Roche, Penzeberg, Germany) were added and the cells were re-incubated for additional 5 hours at 37˚C. Labelling medium was removed by suction and 200 µl/well of FixDenat was added to the cells which were incubated for 30 minutes at room temperature. FixDenat solution is required for the denaturation of the DNA of the cells and later

antibody detection. After removal of FixDenat solution by flicking off and tapping, 100 µl/well of anti-BrdU-POD (monoclonal antibody conjugated with peroxidase) working solution was added and the microplates were incubated for 90 minutes at room temperature.

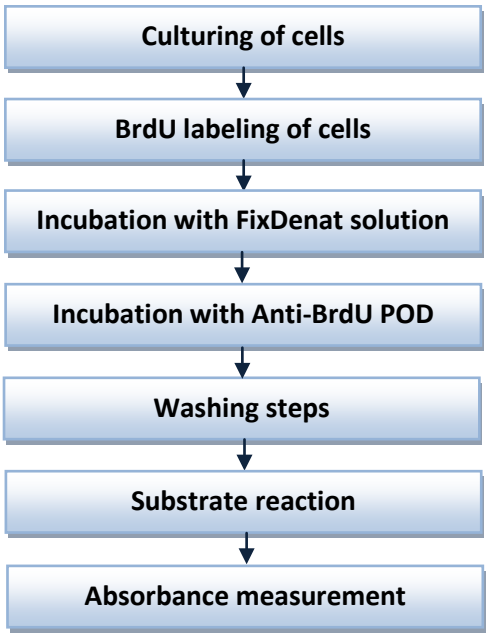

Fig. 7 Steps of BrdU assay protocol

The antibody conjugate was removed by flicking off and the wells were rinsed three times with 200 µl/well Washing solution. Finally 100 µl/well of Substrate solution were added and plates were incubated at room temperature for 15 minutes to reach optimal photometric detection. The absorbance of the samples was measured in an ELISA reader (Multiskan RC, Thermo Labsystems, Finland) at 370 nm. Non treated cells were used as negative control and the results were expressed as an average of five independent experiments. NPs spectrophotometrical interference was estimated performing preliminary readings with:

- PBS
- NPs in PBS
- NPs in PBS and DMEM
- NPs in PBS with anti-BrdU-POD working solution and substrate solution.

3.6 TWO-STAGE CELL TRANSFORMATION ASSAY

The two stage cell-transformation assay was used to simulate the in vivo multistage carcinogenesis. The assay is based on BALB/c 3T3 cells treatment with a sub-threshold dose of a tumor initiator (MCA) at the beginning of cultivation and then with a tumor promoter (TPA) to induce preneoplastic foci.

A tumor promoter, which is a typical non-genotoxic carcinogen, administered individually is not capable to generate foci in 3T3 cells; however, if the cells are treated, at the beginning of cultivation, with an adequate dose of a tumor initiator and later a tumor promoter, a transformation occurs with the proliferation of tumor foci. This type of 2 stage cell transformation (initiation and promotion) assay in vitro is similar to two-stage carcinogenesis in vivo tests [90-91]. The two-stage transformation assay represents an evolution of the "cell transformation assay", developed in 1985 by IARC/NCI/EPA Working Group ", whose purpose was to standardize a method and a device for the study of chemical carcinogens (IARC/NCI/EPA Working Group, 1985).

The two stage transformation assay used to test the NPs was based on the improved method proposed by Kajiwara et al. n 1997 [92]. In particular, it was used a special medium supplemented with a mixture of insulin, transferrin, ethanolamine and sodium selenite (ITES) and a low concentration of fetal bovine serum (FBS). It has been shown that this medium together with MCA+TPA treatment caused high frequency transformation with a high reproducibility. Thanks to this new protocol tumor foci appeared after 45 days instead of the 90 days required by the original protocol.

- ITES cell medium:

Eagle's minimal essential medium (MEM), and Ham F-12 medium and ITES (5000 μg bovine pancreas insulin, 10,000 μg human transferrin, 1530 μg ethanolamine and 4.3 μg sodium selenite in a vial) were obtained from Invitrogen/Life technologies (UK).

Final medium was prepared by mixing an equal volume of MEM medium and Ham F-12 medium with 1% ITES and 5% FBS.

- Protocol:

• $5x10^4$ cells/dish were plated in 60 mm Petri dishes with 5 ml of DMEM medium.

• 24 hours after seeding the cells were treated with the tumor initiator MCA at a concentration of 0.5 μgr/ml. NPs were added at the concentration of 1.5 μgr x 10^6 cells if specified by the layout (see results).

• After three days medium was changed and ITES cell medium was added for another three days.

• Cells were then exposed to the tumor promoter TPA at the concentration of 300 ngr/ml, for two weeks. NPs were added at the concentration of 1.5 μgr x 10^6 cells (see results).

• After two weeks cells were normally seeded with ITES medium for another four weeks.

After foci formation cells were fixed using the following protocol:

• ITES medium was removed from the plates;

• A first quick wash with 100% methanol was executed to rinse the plates from residues;

• 3 ml of 100% methanol were added to the plates for 7 minutes.

• After 7 minutes methanol was discarded and 2 ml of GIEMSA 1:10 stain solution was added to each plate for 5 minutes;

• After 5 minutes the stain was rinsed and the plates were washed with distilled water.

After staining tumor foci count was performed using Media Cybernetics Image-Pro Plus Software.

3.7 NPs MICROSCOPIC MORPHOLOGY AND CHEMICAL COMPOSITION

3.7.1 ENVIRONMENTAL SCANNING ELECTRON MICROSCOPY (ESEM)

Cell NPs interaction was investigated by means of Environmental Scanning Electron Microscopy (ESEM) (ESEM-QUANTA 200 by FEI Company, the Netherlands) combined with an X-ray microprobe of an Energy Dispersive System (EDS, EDAX, USA) (Fig. 8). This instrument is equipped with a Schottky Field Emission Gun (FEG) that provides an optimal lateral resolution of 2 nm.

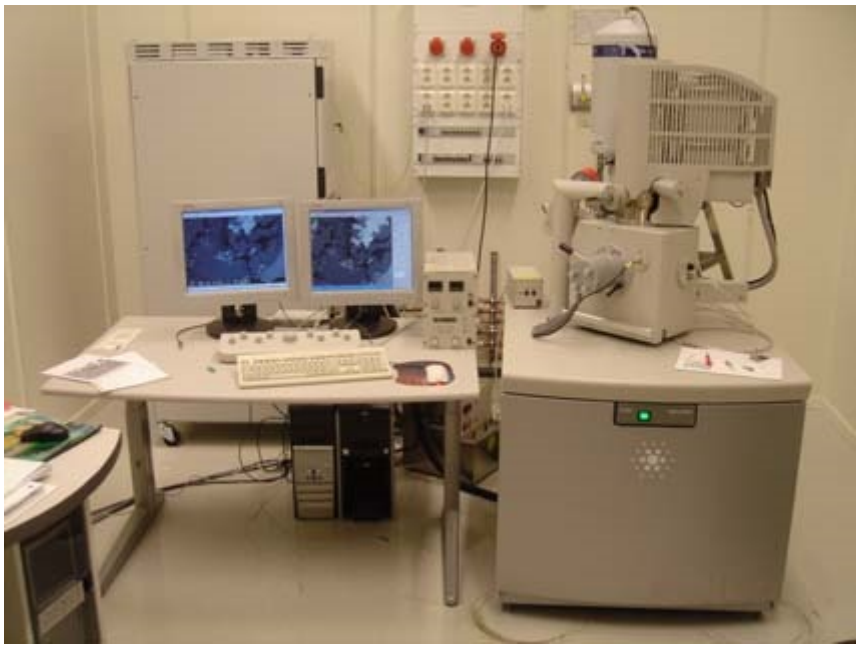

Fig. 8 The Quanta 200 ESEM FEG from FEI.

A scanning electron microscope (SEM) consists of an electron optical column mounted on the top of a specimen chamber maintained in a vacuum system. The electron gun at the top of the optical column produces a focused electron beam directed on the specimen surface (Fig. 9). The secondary and backscattered electrons emitted from the surface due to the primary electron beam are collected by detectors and the resulting signal is amplified and displayed on a computer monitor.

- BSE (BackScatter Electrons) Mode: Backscattered electrons are produced by the elastic interactions between the sample and the incident electron beam. The energy generated is comparable to that of the incident electrons and it's proportional to the sample's atomic number, or more exactly, BSE images show difference in composition. The higher the atomic numbers of the

element, the more backscattered electrons are detected, making the image brighter for larger atoms. This mode provides image contrast as a function of elemental composition.

- SEC (SECondary Electrons) Mode: Inelastic electron scattering caused by the interaction between the sample's electrons and the beam's incident electrons results in the emission of low-energy electrons that overcome the surface energy barrier and escape from the sample. These electrons are known as secondary electrons and are produced both by the incoming primary electrons and by the escaping backscattered electrons.. The local variation in secondary electron intensity is used to create the image contrast that reveals the surface morphology and its texture. The more the number of electrons reaching the detector, the brighter the image is. Furthermore SEC mode provides high-resolution imaging of fine sample topography with a detectable limit of few nanometers.

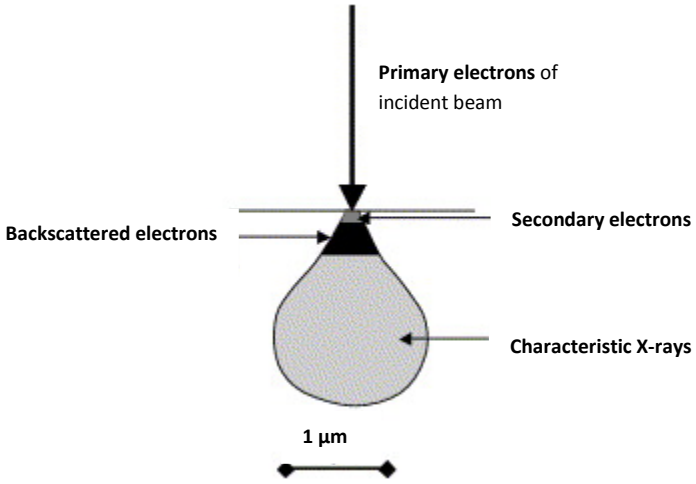

Fig. 9 The typical spatial resolution of different signals in ESEM mode: secondary electrons, backscattered electrons and X-rays.

Environmental Scanning Electron Microscopy (Fig. 8) can deliver various kinds of information:

1. Topography: the surface features of the sample and its texture.
2. Morphology: the shape, size and arrangement of the particles making up the objects that are lying on the surface of the sample or have been exposed by grinding or chemical etching.
3. Composition: the elements and compounds the sample is composed of and their relative ratios.
4. Crystallographic Information: the arrangement of atoms in the specimen and their degree of order; only useful on single-crystal particles >20 micrometers.

With the ESEM instrument, it is possible to analyze samples at room conditions and to observe wet and oily materials without prior dehydration of the samples or to deposit an electron-conductive layer on their surface. As no sample preparation is needed, the ESEM observations provide detailed images of the real morphology of organic and inorganic matter without any contamination or specimen's alteration.
Thanks to the possibility to observe cells without any treatment and any further process altering morphology, location, cell membrane integrity etc., the NPs-cell interaction was deeply investigated.

Protocol:

Cells were cultured at a density of $6x10^4$ cells/well in 12-well plates, in which a 13-mm diameter plastic coverslip (Thermanox Plastic Coverslips, NUNC, USA) had been placed.

Cells were treated with NPs at the dilution of 1.5 µg/10^6 cells for 48/72h. Thereafter, treated and untreated (control) cells were extensively washed with PBS buffer, fixed in a 4% glutaraldehyde solution for 1h and dehydrated in ascending concentration solutions of ethanol (70, 90, 100%) for 10 minutes. The cells were observed in low vacuum modality in order to preserve cells samples and without further treatments or manipulations.

3.7.2 ENERGY DISPERSIVE X-RAY SPECTROSCOPY

An elemental analysis of NPs was performed using an X-ray microprobe of an Energy Dispersive Spectroscopy (EDS) (EDS by EDAX, USA), in order to verify the chemical composition of the NPs. Characteristic X-rays generated from a microscopic volume in spot mode (i.e., beam not scanning) are utilized to obtain a complete quantitative chemical analysis.

The energy of each X-ray photon is characteristic of the element which produced it. The EDS microanalysis system collects the X-rays, sorts and plots them by energy, and automatically identifies and labels the elements responsible.

A typical EDS spectrum is displayed as a plot of x-ray counts vs. energy (in keV). Energy peaks correspond to the various elements in the sample (Fig. 10).

Identifying the specific energy of the characteristic x-ray peaks for each element and comparing EDS data to computer-generated standards, it is possible to perform a qualitative analysis.

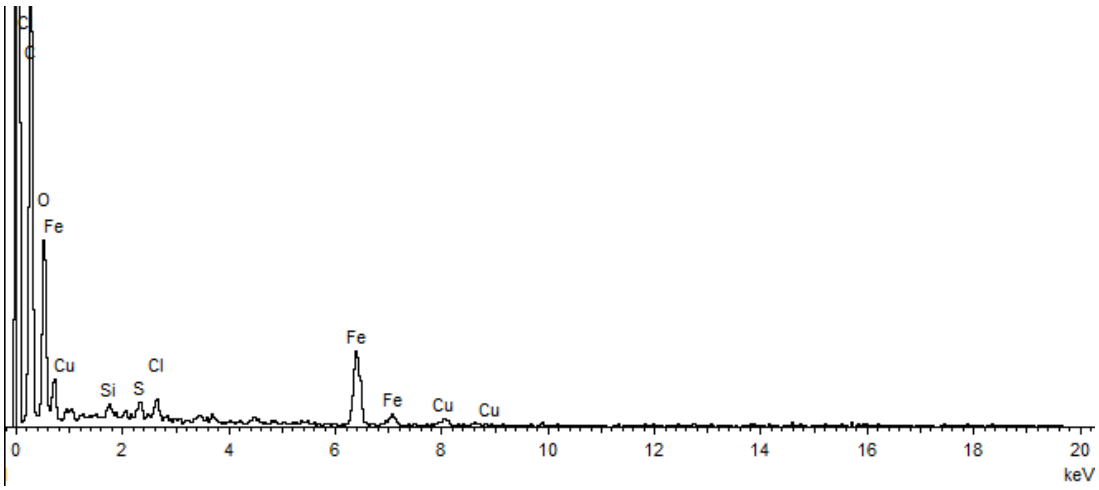

Fig. 10 Example of EDS spectrum

3.8 STATISTICAL ANALYSIS

The significance of the results was evaluated using GraphPad Prism 5 software.

Statistical analysis of variance (ANOVA) and the comparative test of Dunnet (p value 0.05 <) were applied to all the acquired data.

4. RESULTS

4.1 NANOPARTICLES CHARACTERIZATION

DLS analyzes were performed to obtain information on NPs average diameter and aggregation state in solution (DMEM) at the concentration of 0,025 μg/ml. Significant problems occurred during the sample preparation, with the formation of dry NPs aggregates upon suspension in cell culture medium. Aggregates were partially dissolved by sonication and filtered through a 0.8 μm filter. After treatment NPs better volume distribution and quality analyses were obtained (PDI=1). The data are shown in table 7.

NPs	**Average Diameter (nm) in DMEM**				
	1 min	**30 min**	**24h**	**48h**	**72h**
Au	116 ± 24.9	129 ± 18.2	190 ± 10.1	117 ± 20.1	120 ± 28.6
Co	187 ± 15.1	103 ± 16.1	122 ± 11.3	141 ± 11.2	134 ± 12.4
Fe_3O_4	139 ± 24.5	145 ± 12.6	161 ± 12.4	159 ± 15.7	178 ± 11.7
CeO_2	178 ± 12.1	173 ± 21.2	121 ± 21.1	175 ± 19.8	188 ± 17.3

Tab. 7 DLS results of NPs size.

Negative Z-Potential values (related to surface charge) were observed in general for all the four different NPs. Data are shown in table 8.

	Z-Potential (mV)
DMEM	-18,7
Au	-10
Co	-8,20
Fe_3O_4	-10,6
CeO_2	-8,48

Tab. 8 Zeta potential measurements.

TEM and ESEM results of gold, iron oxide, and cerium oxide NPs confirmed the tendency of the NPs to aggregate and to form clusters (Fig.11-12).

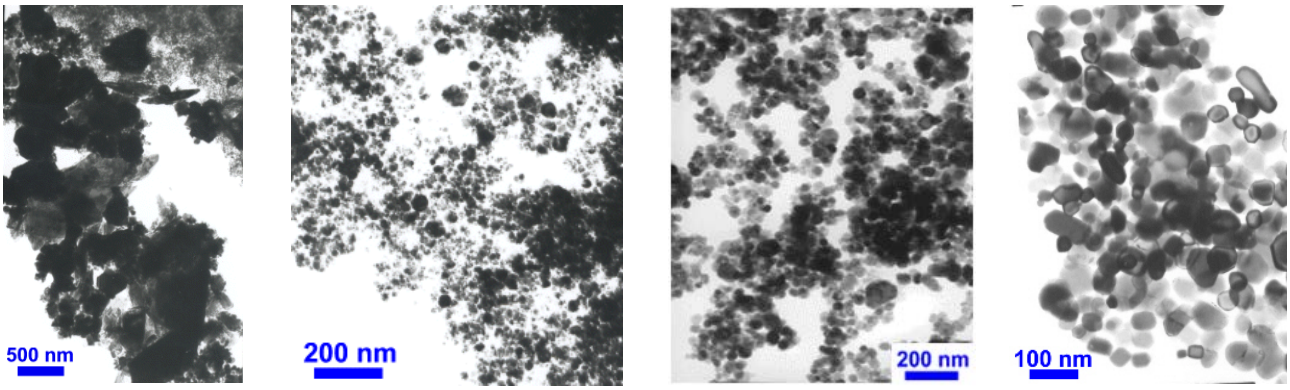

Au Co Fe_3O_4 CeO_2

Fig. 11 TEM images and characterization of the various NPs.

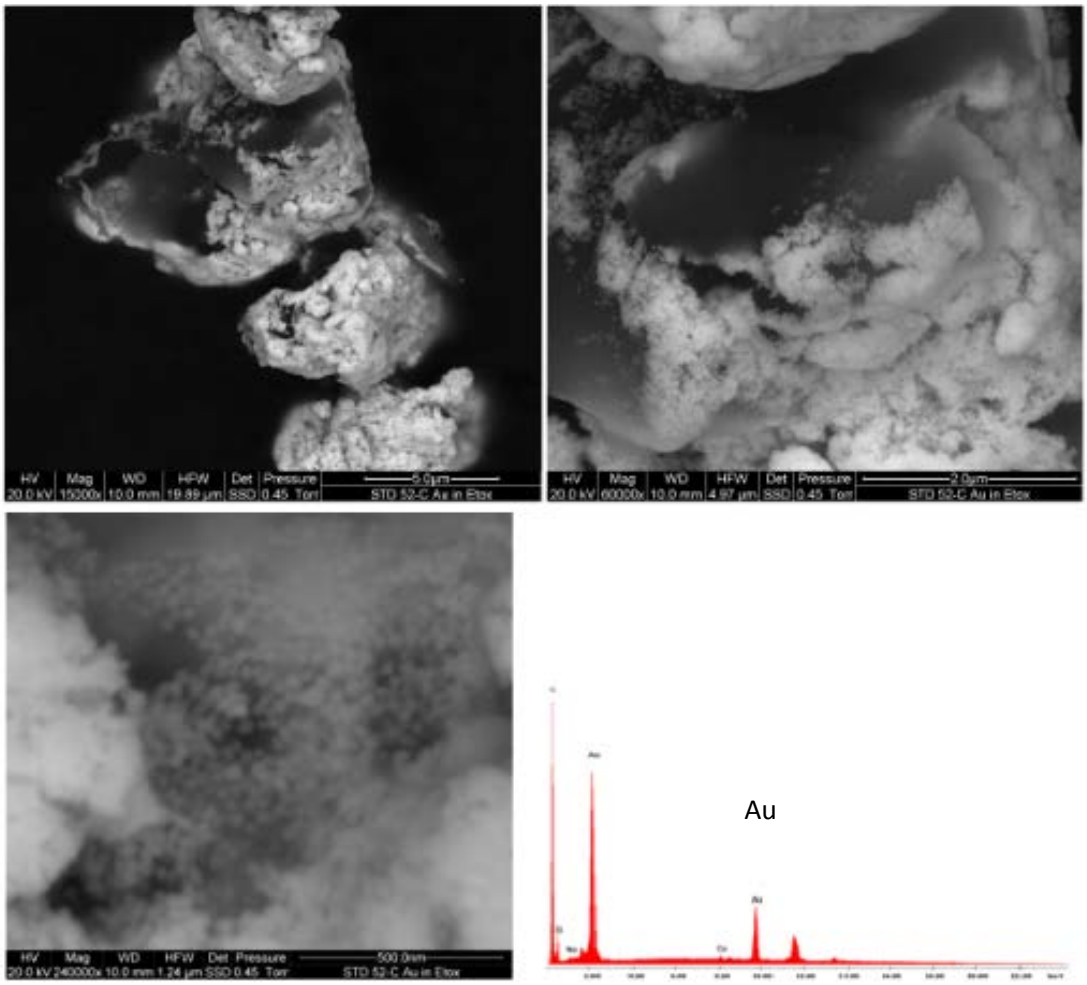

Fig. 12 ESEM images of Au NPs (240.000x) and relative EDS spectrum.

4.2 XTT CELL VIABILITY RESULTS

Cell viability was measured after NPs exposure on the SHSY-5Y, U-87 and BV-2 cell lines and on the rat primary cells, using XTT assay (Cell viability Kit II -XTT, Roche, Mannheim, Germany). The cytotoxicity studies were performed in triplicate for each population in order to verify the results reproducibility after 48-72h. Data were statistically analyzed and are expressed in the graphs as mean ± standard deviation by application of ANOVA model. Non treated cells were used as negative control. The data plotted in the graphs are relative to NPs sub toxic dilution of 1.5 μg x 10^6 NPs/cells and was estimated after initial dose response curves.

4.2.1 XTT RESULTS ON SH-SY5Y CELLS

After 48h of exposure to the four types of metal NPs, SH-SY5Y cells showed a reduction in cell viability (Fig. 13). At 48 hours the NPs of iron oxide and gold showed a decrease of cell vitality by over 16% relative to the control, and in the case of cobalt NPs and cerium oxide reduction reaches about 32%. After 72 hours of treatment, cell viability is slightly reduced only after cobalt NPs treatment.

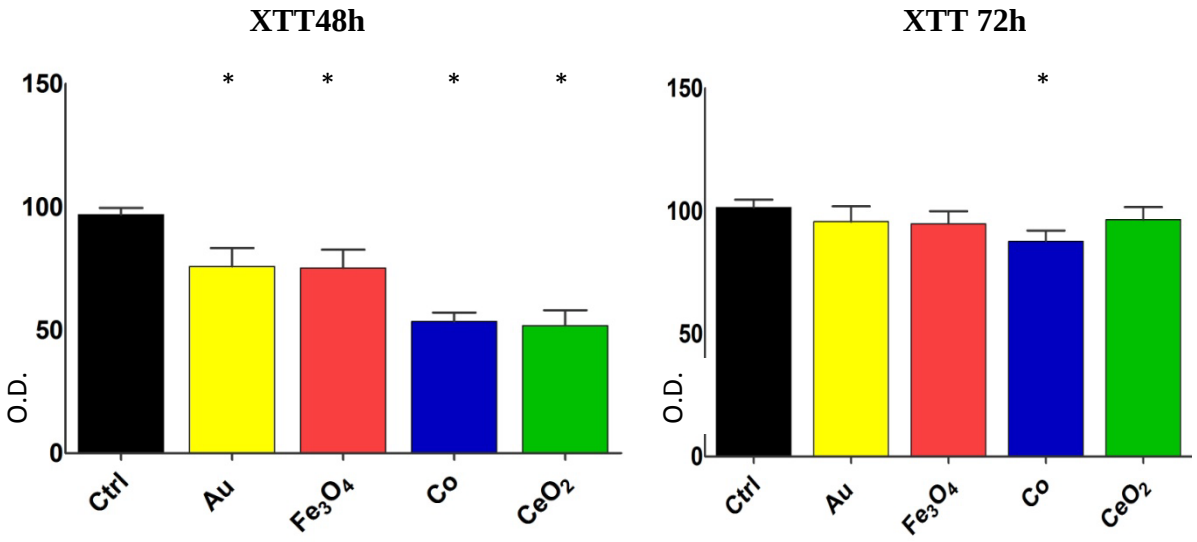

Fig. 13 XTT assay on SH-SY5Y cells after NPs treatment at 48h and 72h (* p< 0,05, O.D.= Optical Density %).

4.2.2 XTT RESULTS ON U-87 CELLS

U-87 cells showed a decrease in viability after treatment with NPs of iron oxide, cobalt oxide and cerium oxide at both 48 and 72h (Fig. 14).

Cobalt NPs caused a 41% decrease in cell viability after 48/72 hours of exposure. Cerium oxide NPs reduced by 30% the cell viability after 48 hours of contact. At 72 hours cerium oxide NPs decreased cell viability down to -39%.

On the contrary gold NPs showed a slight increase in cell viability after 48h but not at 72h.

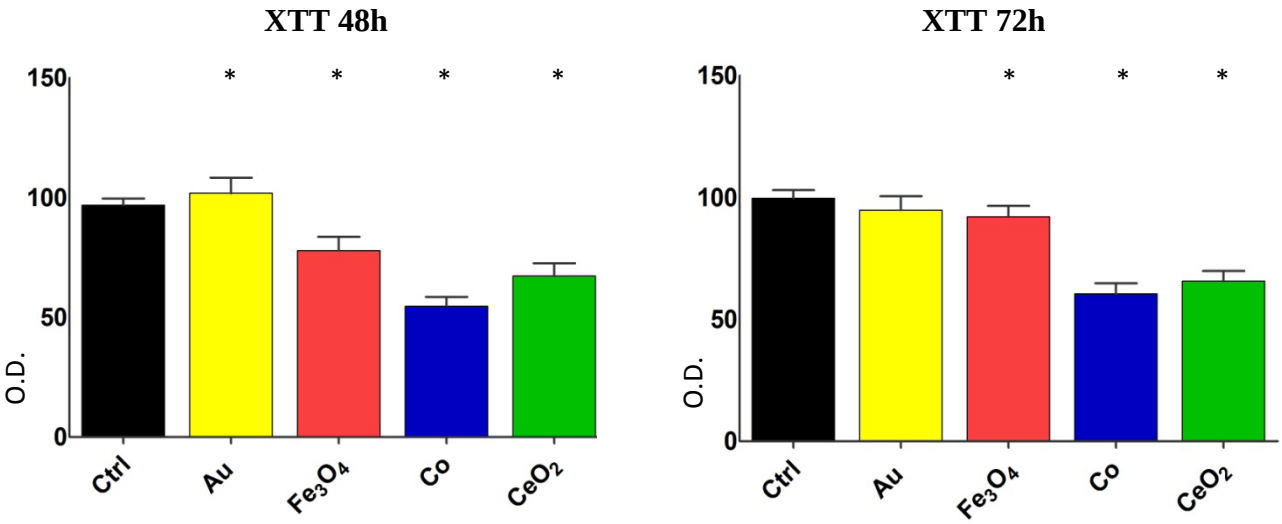

Fig.14 XTT assay on U-87cells after NPs treatment at 48h and 72h (* p< 0,05, O.D.= Optical Density %).

4.2.3 XTT RESULTS ON BV-2 CELLS

BV-2 cells did show an increase in cell viability after exposure to gold and iron oxide NPs at 48h (Fig. 15). No decrease in cell viability was found after exposure to cobalt and cerium oxide NPs at both 48 and 72h despite the large presence of the particles inside the cells due to phagocytosis. At 72h no significant alterations of cell viability were found.

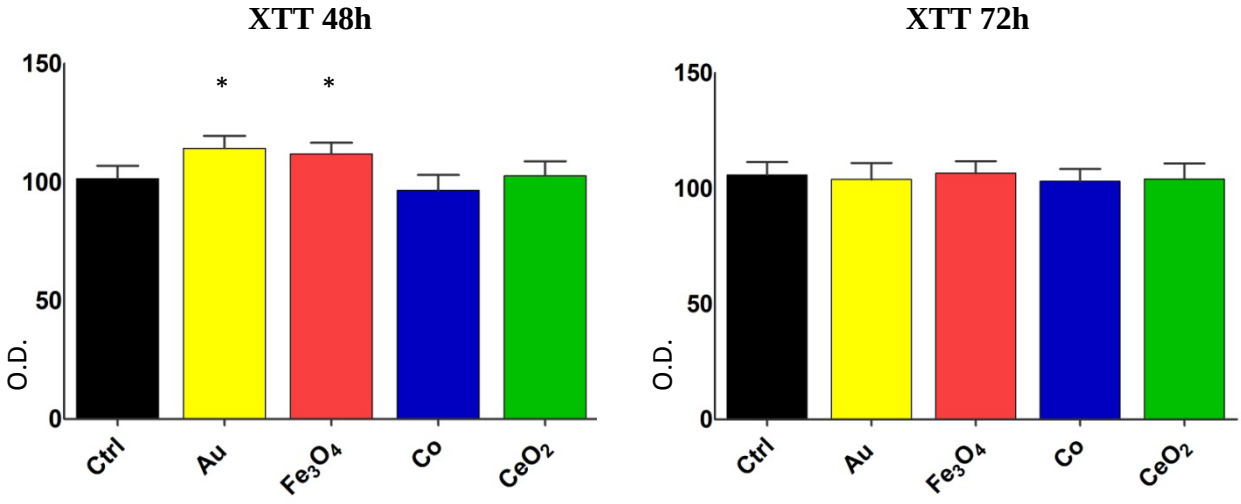

Fig.15 XTT assay on BV-2 cells after NPs treatment at 48h and 72h (* p< 0,05, O.D.= Optical Density %).

4.2.4 XTT RESULTS ON RAT PRIMARY CELLS

No significant decline in cell viability after 48/72h of exposure to NPs in both Rat primary cells sub population (glial cells and neurons) was found (Fig. 16). Selective uptake on glial cells was demonstrated by ESEM morphological analyzes although no variations in mitochondrial cell metabolism was significantly detected. Rat primary cells have a slow functionality which may require an over 72h NPs time of exposure.

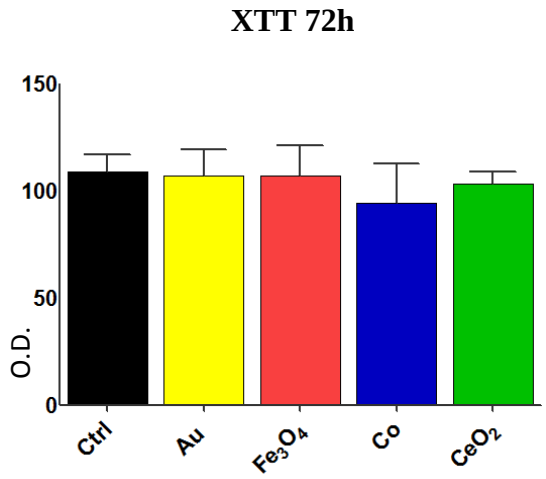

Fig.16 XTT assay on Rat primary cells after NPs treatment at 72h (* p< 0,05, O.D.= Optical Density %).

4.3 BrdU CELL PROLIFERATION RESULTS

Cell proliferation was measured using BrdU ELISA assay after 48/72h NPs exposure on the SHSY-5Y, U-87 and BV-2 immortalized cell lines. Primary cells do not proliferate therefore no cell proliferation was tested on glial and neuronal rat primary cells. Data were statistically analyzed and are expressed in the graphs as mean ± standard deviation by application of ANOVA model. Non treated cells were used as negative control. The data plotted in the graphs are relative to NPs sub toxic dilution of 1.5 μg x 10^6 NPs/cells and was estimated after initial dose response curves.

4.3.1 BrdU ELISA RESULTS ON SH-SY5Y CELLS

Similarly to the XTT data, SH-SY5Y cells showed a decrease in cell proliferation after 48h of contact with all types of NPs (Fig. 17).

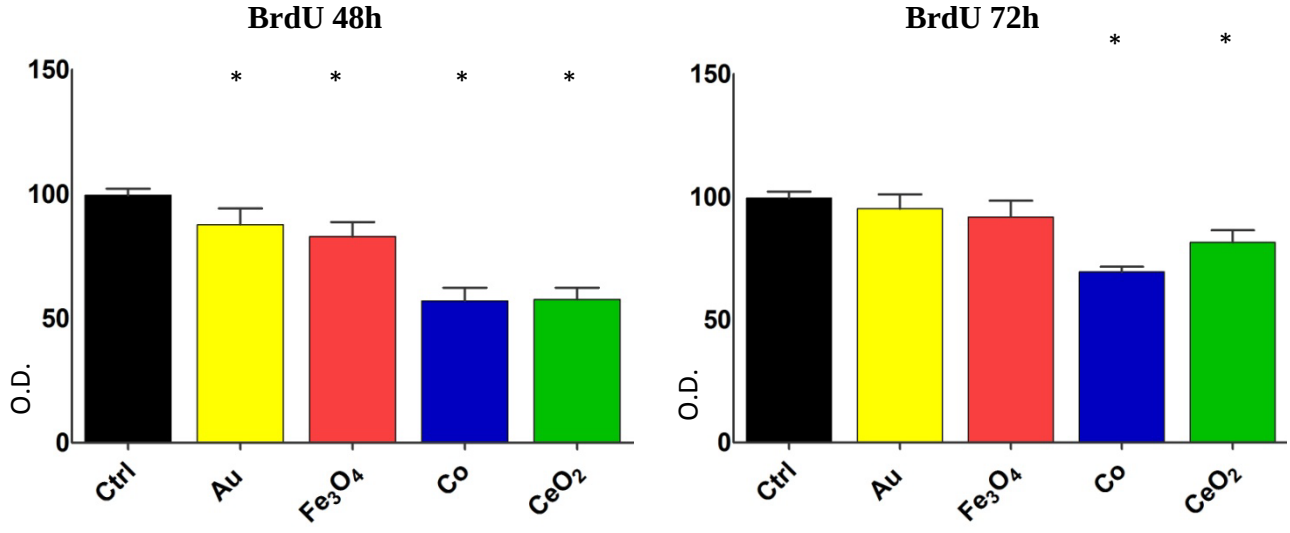

Fig.17 BrdU ELISA on SH-SY5Y cells after NPs treatment at 48h and 72h (* p< 0,05, O.D.= Optical Density %).

At 48 hours iron oxide and gold NPs caused a decrease of cell proliferation by over 12% relative to the control. Cobalt NPs and cerium oxide NPs decreased cell proliferation by 47%. After 72 hours of treatment, cell proliferation is reduced only after cobalt (38%) and cerium oxide (17%) NPs treatment.

4.3.2 BrdU ELISA RESULTS ON U-87 CELLS

At 48 hours U-87 cells showed a significant decrease in cell proliferation only after contact with cobalt and cerium oxide NPs (Fig. 18). Cobalt and cerium oxide NPs decreased cell proliferation by 39%. After 72 hours of treatment, cell proliferation is reduced only after cobalt (7-8%) NPs treatment.

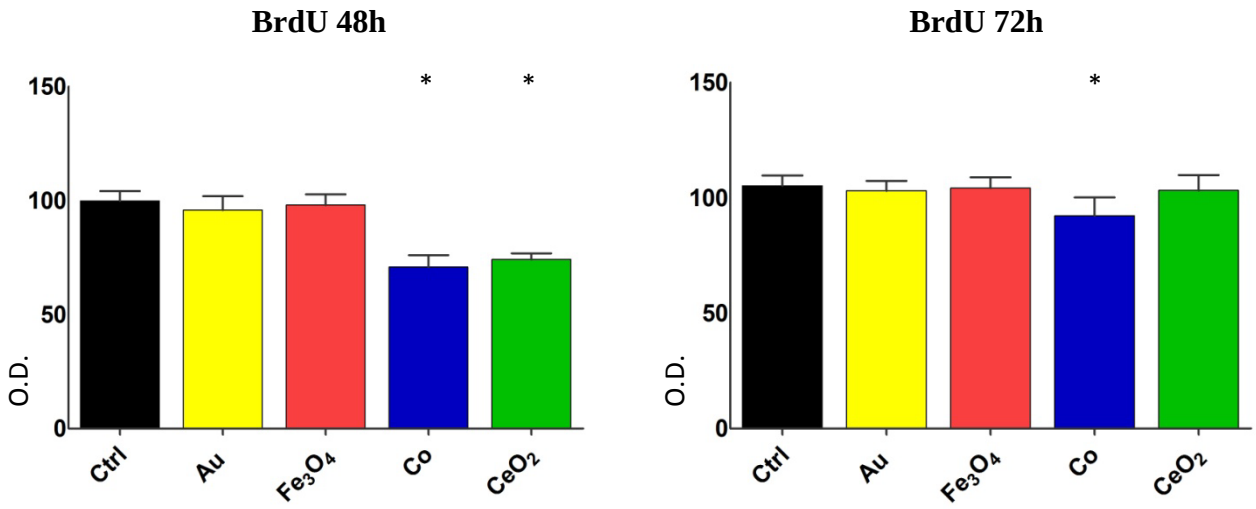

Fig.18 BrdU ELISA on U-87 cells after NPs treatment at 48h and 72h (* p< 0,05, O.D.= Optical Density %).

4.3.3 BrdU ELISA RESULTS ON BV-2 CELLS

After 48/72 hours of NPs treatment no significant alterations of BV-2 cell proliferation were found despite the large number of particles swallowed by phagocytosis (Fig. 19).

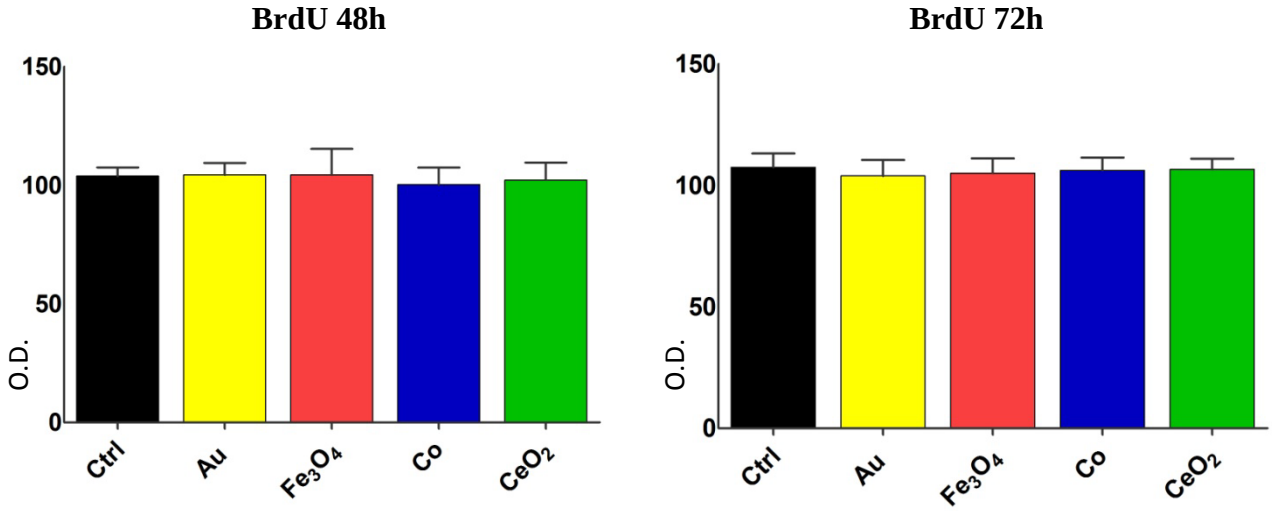

Fig.19 BrdU ELISA on BV-2 cells after NPs treatment at 48h and 72h (* p< 0,05, O.D.= Optical Density %).

4.4 ESEM ANALYZES

Cell morphology before and after the NPs interaction was evaluated using ESEM microscopy. The identification of the NPs on the cell surface was clearly seen on all the analyzed cell lines. NPs localization was pronounced on BV-2 immortalized cells and in mouse primary glial cells. Using micro EDS analysis it was possible to confirm the chemical composition of the NPs obtaining both qualitative and quantitative data on their presence.

4.4.1 SH-SY5Y ESEM ANALYZES

ESEM analysis of SH-SY5Y cells after 48 hours of contact with the NPs showed a close interaction between the NPs and neuronal cells (Fig. 20-24). Neuroblastoma cell morphology was well preserved (Figure 21) and the presence of aggregates of particles of various sizes on the surface was verified. Using electron back scattered mode it was possible to identify the possible particle uptake into the cytoplasm. NPs were detected in clusters and non homogeneously distributed.

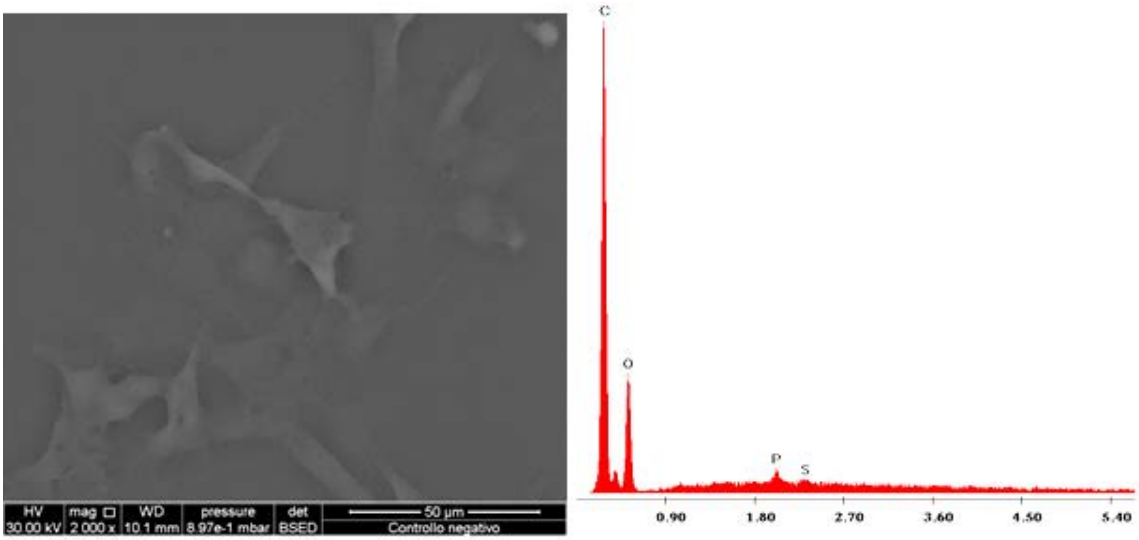

Fig. 20 ESEM image of SH-SY5Y cells without any treatment - 2000x. On the right the basal EDS spectrum is reported.

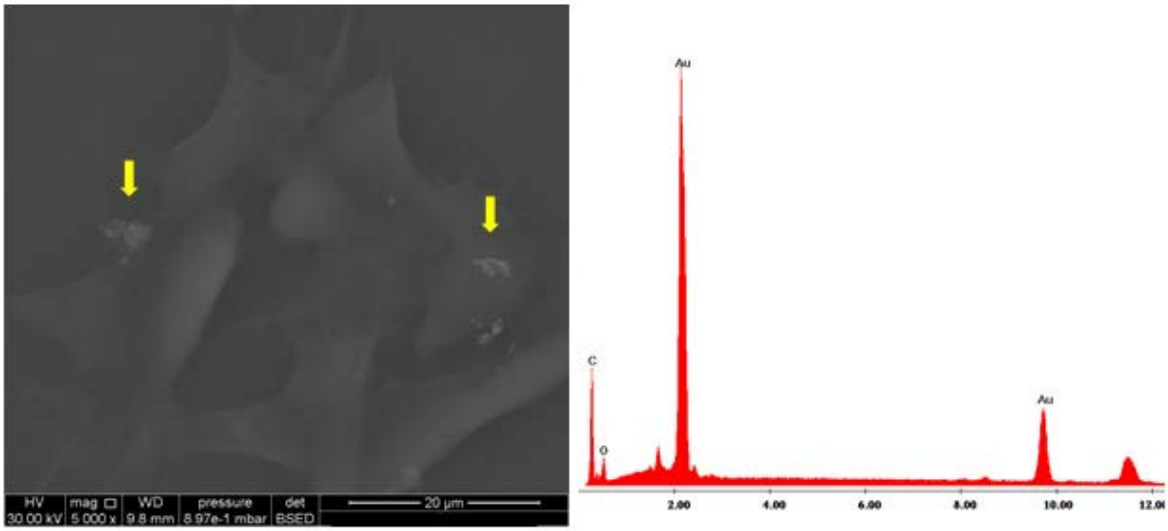

Fig. 21 ESEM image of SH-SY5Y cells exposed to NPs of gold (the arrows indicate the presence of Au NPs) - 5000x. On the right the EDS spectrum of the Au NPs is reported.

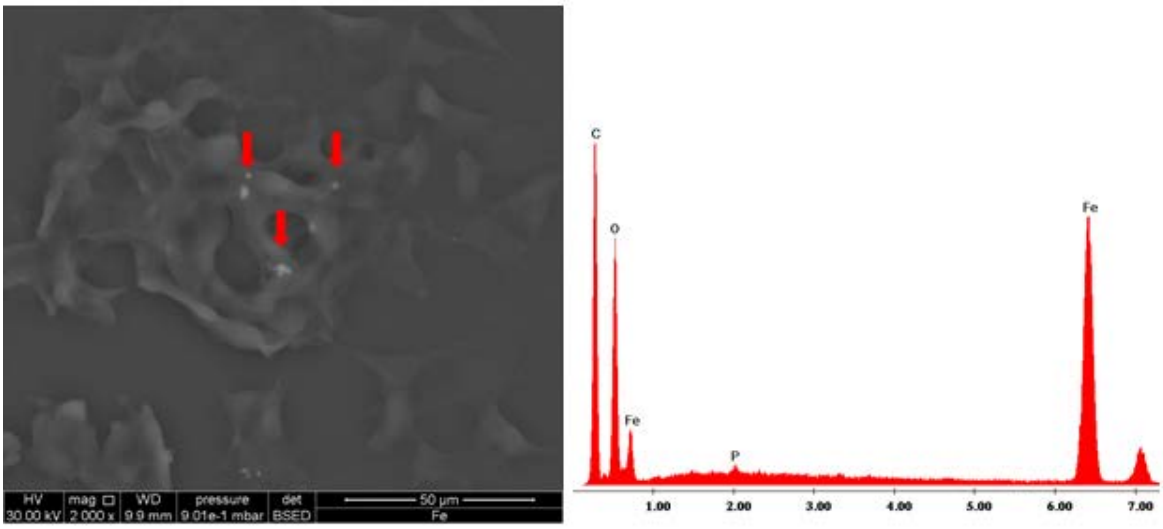

Fig. 22 ESEM image of SH-SY5Y cells exposed to iron oxide NPs (the arrows indicate the presence of NPs) - 2000x. On the right the EDS spectrum of the Fe_3O_4 NPs is reported.

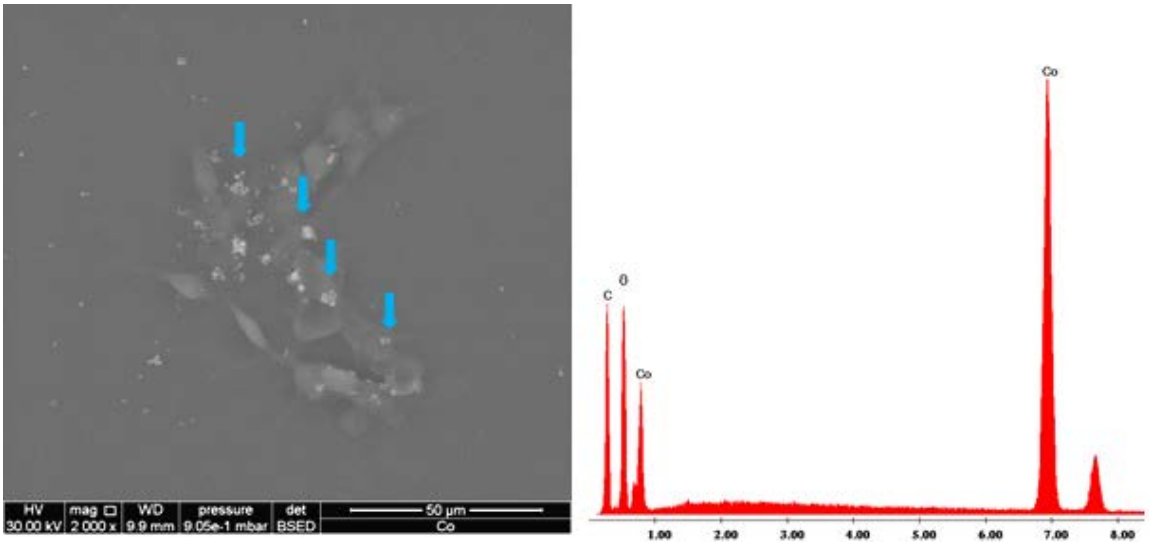

Fig. 23 ESEM image of SH-SY5Y cells exposed to cobalt NPs (the arrows indicate the presence of NPs) - 2000x. On the right the EDS spectrum of the Co NPs is reported.

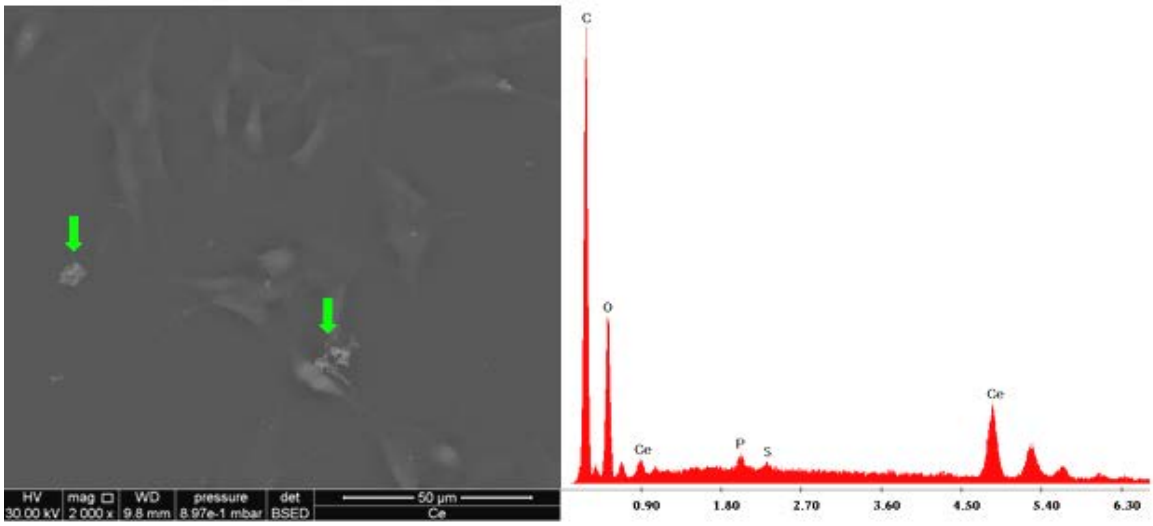

Fig. 24 ESEM image of SH-SY5Y cells exposed to cerium oxide NPs (the arrows indicate the presence of NPs) - 2000x. On the right the EDS spectrum of the CeO_2 NPs is reported.

4.4.2 U-87 ESEM ANALYZES

Morphological analysis of U-87 cells after 48 hours of contact with each of the four nanoparticle types confirmed a close interaction between the particles and cells (Fig. 25-29). NPs uptake was found to be higher in U-87 cells than in SH-SY5Y. In general NPs were detected in clusters and non homogeneously distributed. U-87 glioblastoma cells were found well adherent to the support and maintained their typical morphology despite the superficial or internal presence of the NPs. The cell apparently did not show any signs of suffering and the particles were present as singlet or aggregates. EDS spectrum confirmed the composition of the particles observed.

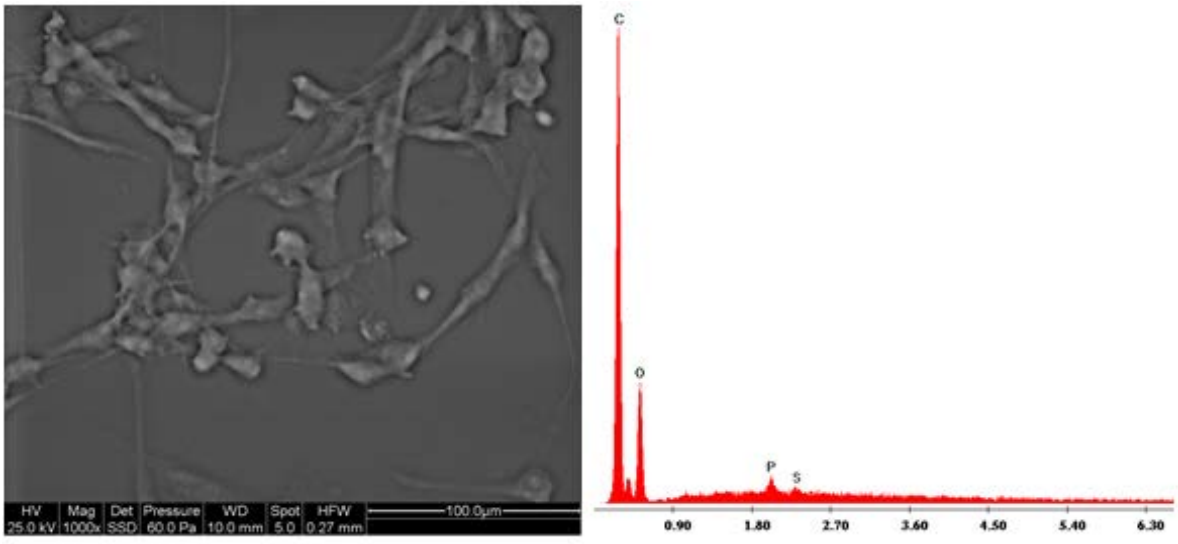

Fig.25 ESEM image of non treated U-87 cells 1000x. On the right basal EDS spectrum is reported.

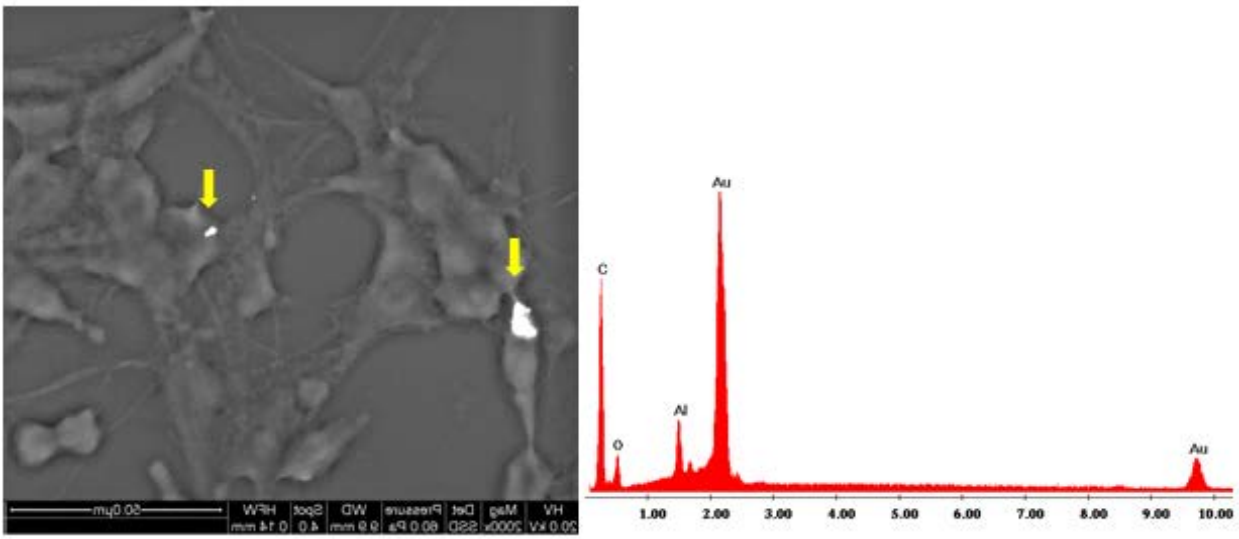

Fig.26 ESEM image of U-87 cells exposed to NPs of gold (the arrows indicate the presence of NPs) - 2000x. On the right the EDS spectrum of the Au NPs is reported.

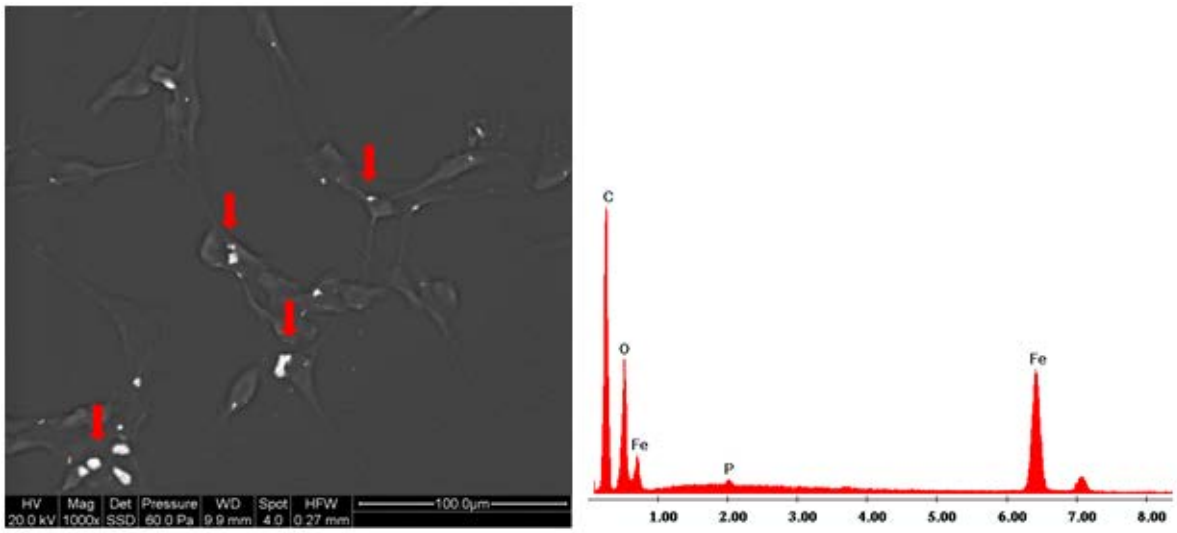

Fig.27 ESEM image of U-87 cells exposed to Iron oxide NPs (the arrows indicate the presence of NPs) - 1000x. On the right the EDS spectrum of the Fe_3O_4 NPs is reported.

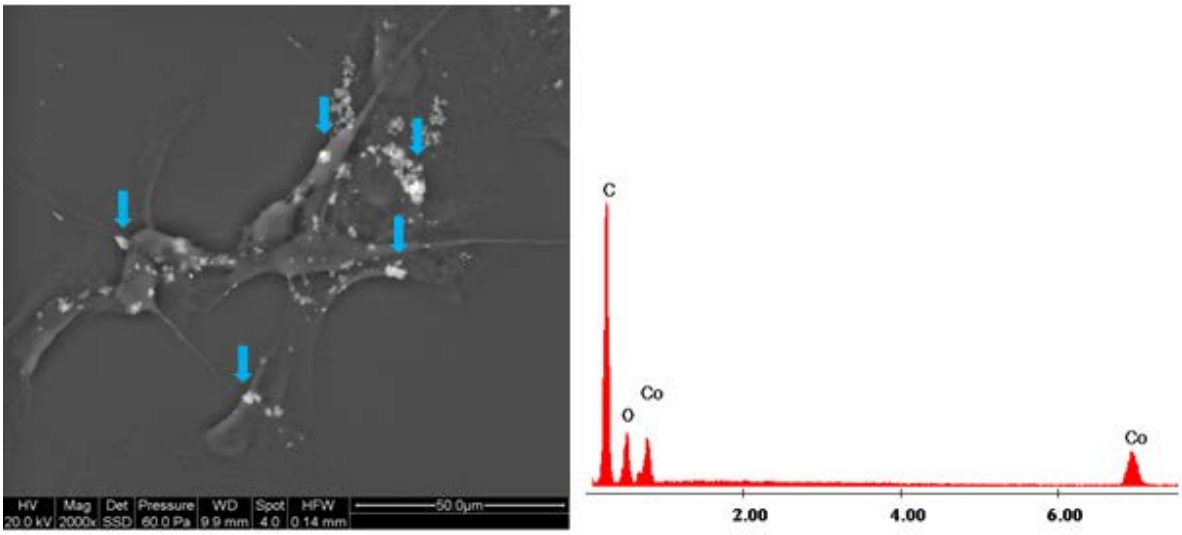

Fig.28 ESEM image of U-87 cells exposed to cobalt NPs (the arrows indicate the presence of NPs) - 2000x. On the right the EDS spectrum of the Co NPs is reported.

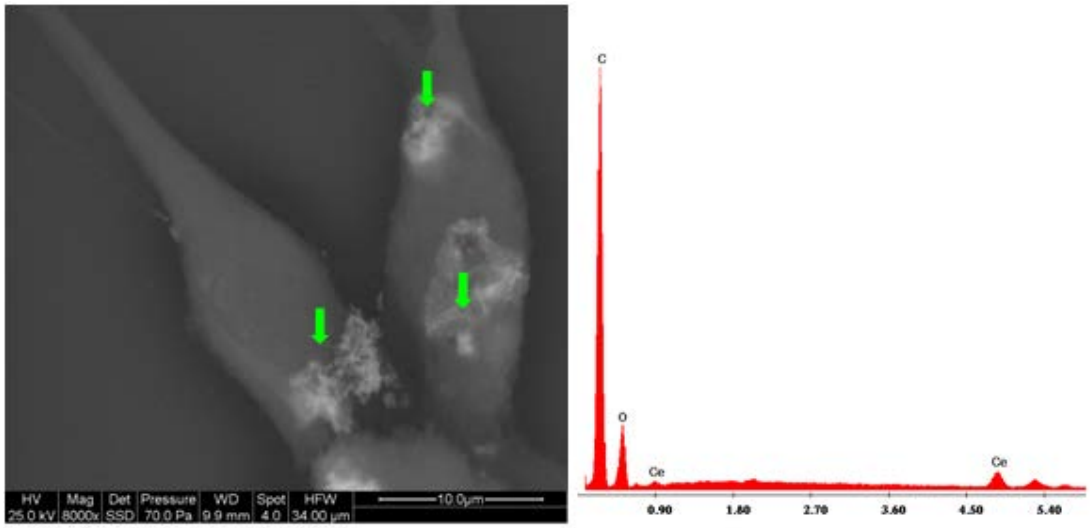

Fig.29 ESEM image of U-87 cells exposed to cerium oxide NPs (the arrows indicate the presence of NPs) - 1000x. On the right the EDS spectrum of the CeO_2 NPs is reported.

4.4.3 BV-2 ESEM ANALYZES

ESEM analysis of BV-2 cells after 48 hours of contact with the NPs showed an high interaction between the NPs and the microglia cells. Using electron backscattered mode it was possible to identify the activity of the microglia cells: BV-2 cells were able to internalize by phagocytosis most of the particles (Fig. 30-34). BV-2 cell morphology was preserved presenting a slightly enlarged cytoplasm with swollen NPs.

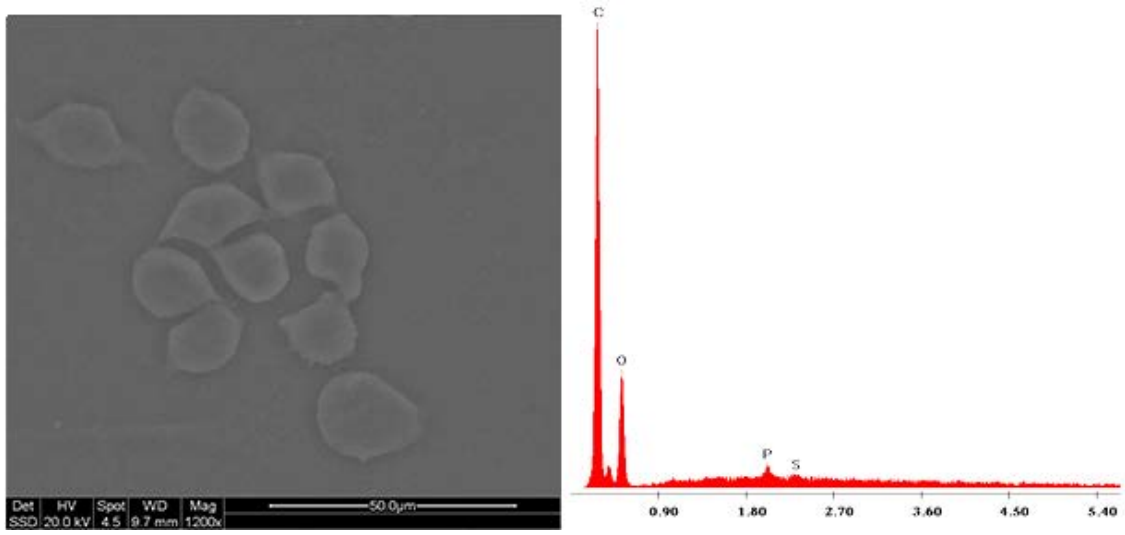

Fig. 30 ESEM image of BV-2 cells without any treatment - 1200x. On the right the basal EDS spectrum is reported.

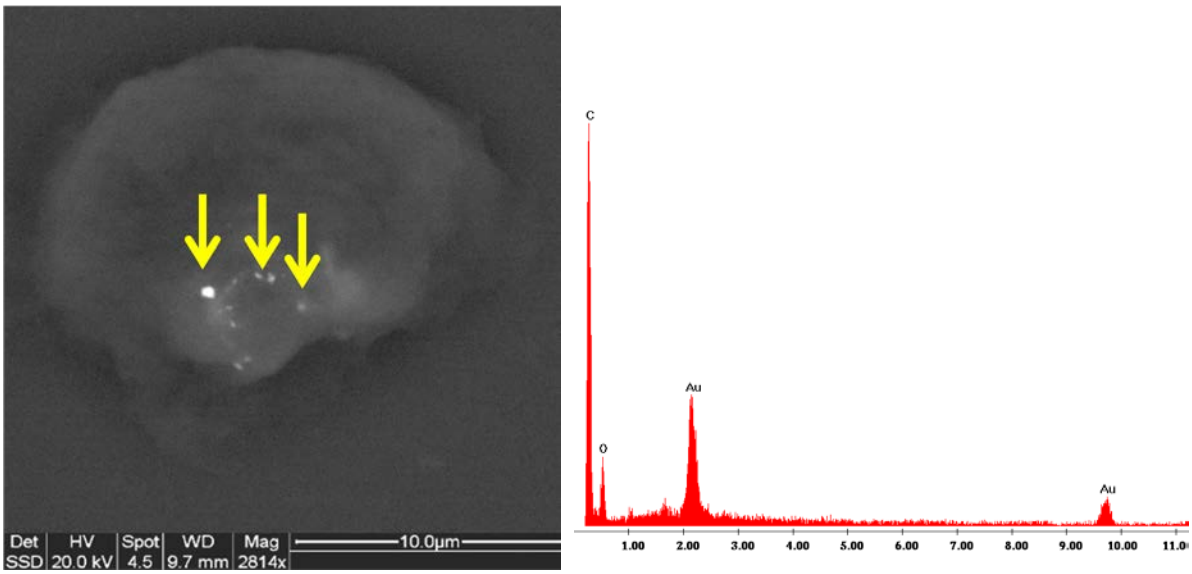

Fig. 31 ESEM image of BV-12 cells exposed to NPs of gold (the arrows indicate the presence of NPs) - 5000x. On the right the EDS spectrum of the Au NPs is reported.

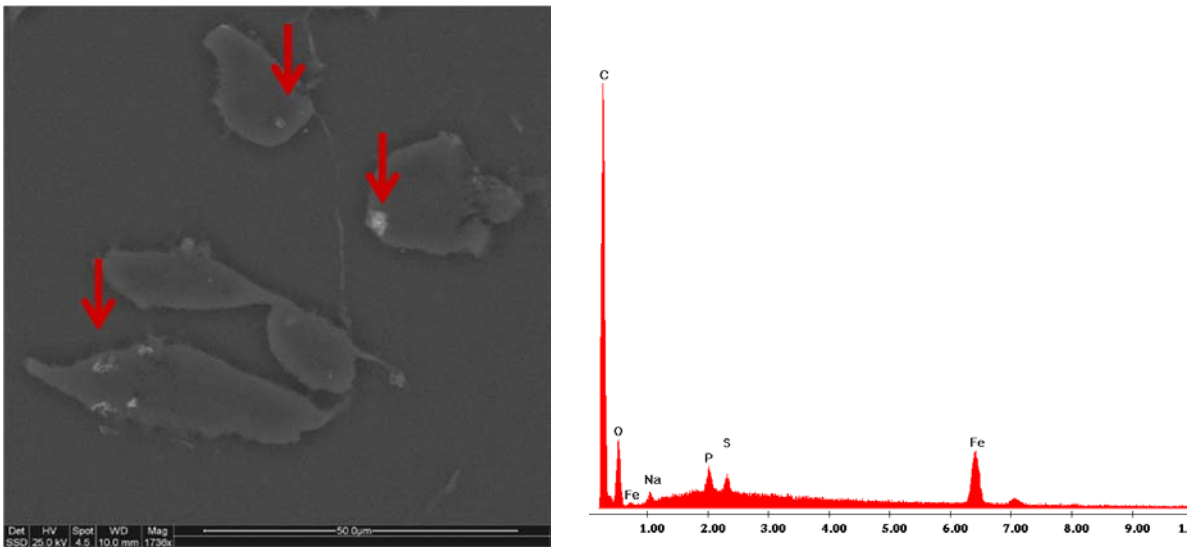

Fig. 32 ESEM image of BV-2 cells exposed to iron oxide NPs (the arrows indicate the presence of NPs) - 2000x. On the right the EDS spectrum of the Fe_3O_4 NPs is reported.

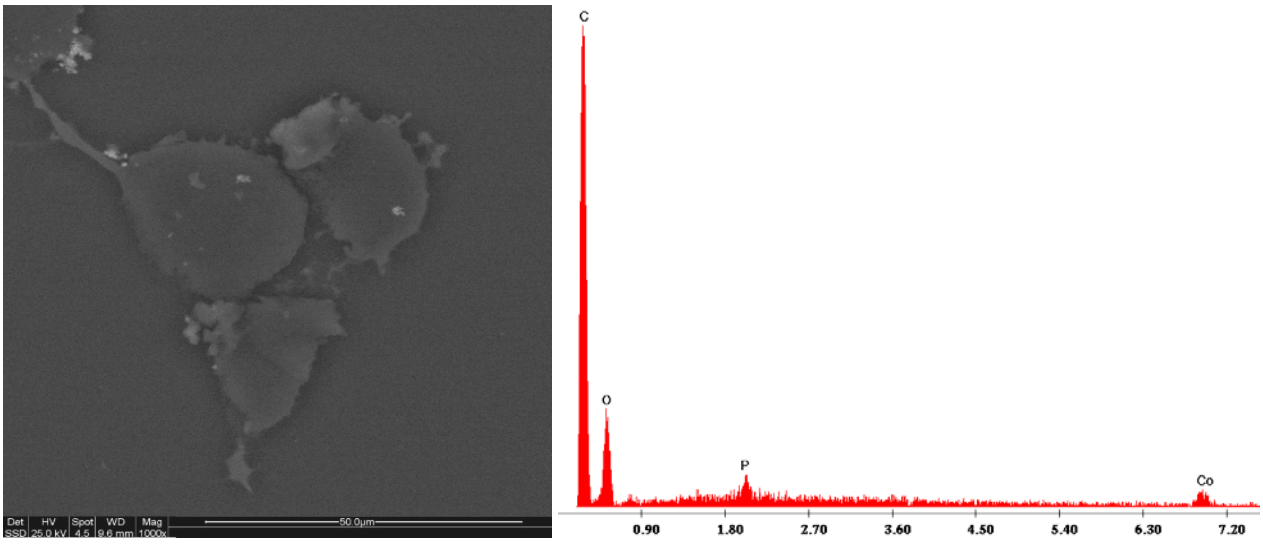

Fig. 33 ESEM image of BV-2 cells exposed to cobalt NPs (the arrows indicate the presence of NPs) - 2000x. On the right the EDS spectrum of the Co NPs is reported.

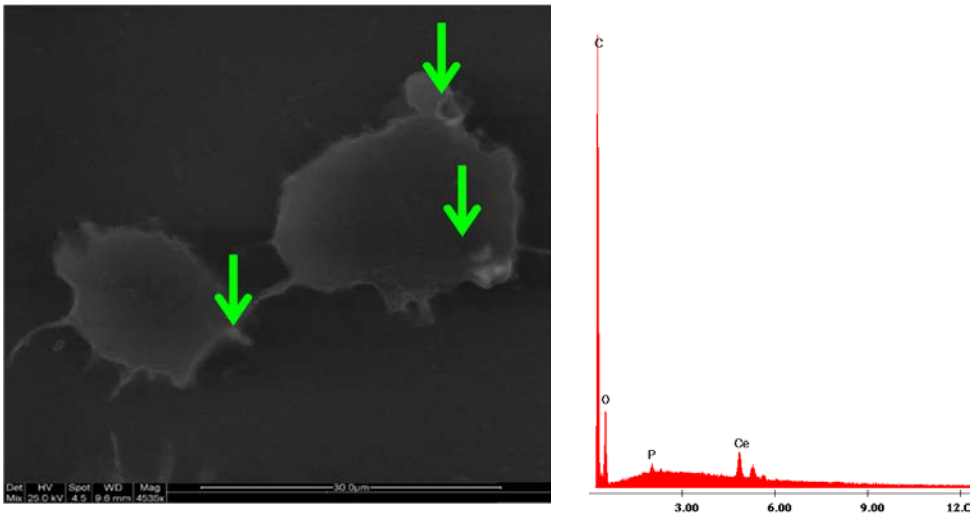

Fig. 34 ESEM image of BV-2 cells exposed to cerium oxide NPs (the arrows indicate the presence of NPs) - 2000x. On the right the EDS spectrum of the CeO_2 NPs is reported.

4.4.4 ESEM ANALYZES OF RAT PRIMARY CELL CULTURES

In rat primary cultures (Fig. 35), glial cells sub population showed a large cytoplasmatic uptake of NPs whereas neurons revealed a lower internalization (backscattered electron mode). In addition, gold and iron oxide NPs apparently increased glial cells membranes volume (Fig. 36-37). On the contrary, all the primary subpopulations cells in contact with cobalt and cerium oxide did not show morphological alterations. The distribution of NPs was found not homogeneous; clusters of particles of different sizes are present both in the glial cells that neural connections.

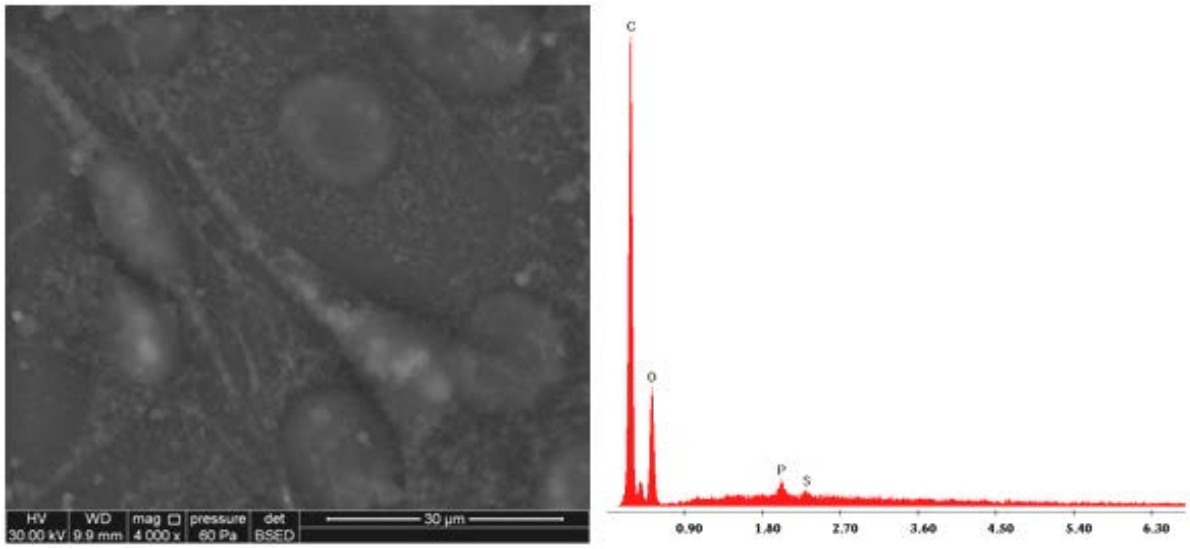

Fig.35 ESEM image of rat primary cells - neurons and glia - without any treatment - 4000x. On the right the basal EDS spectrum is reported.

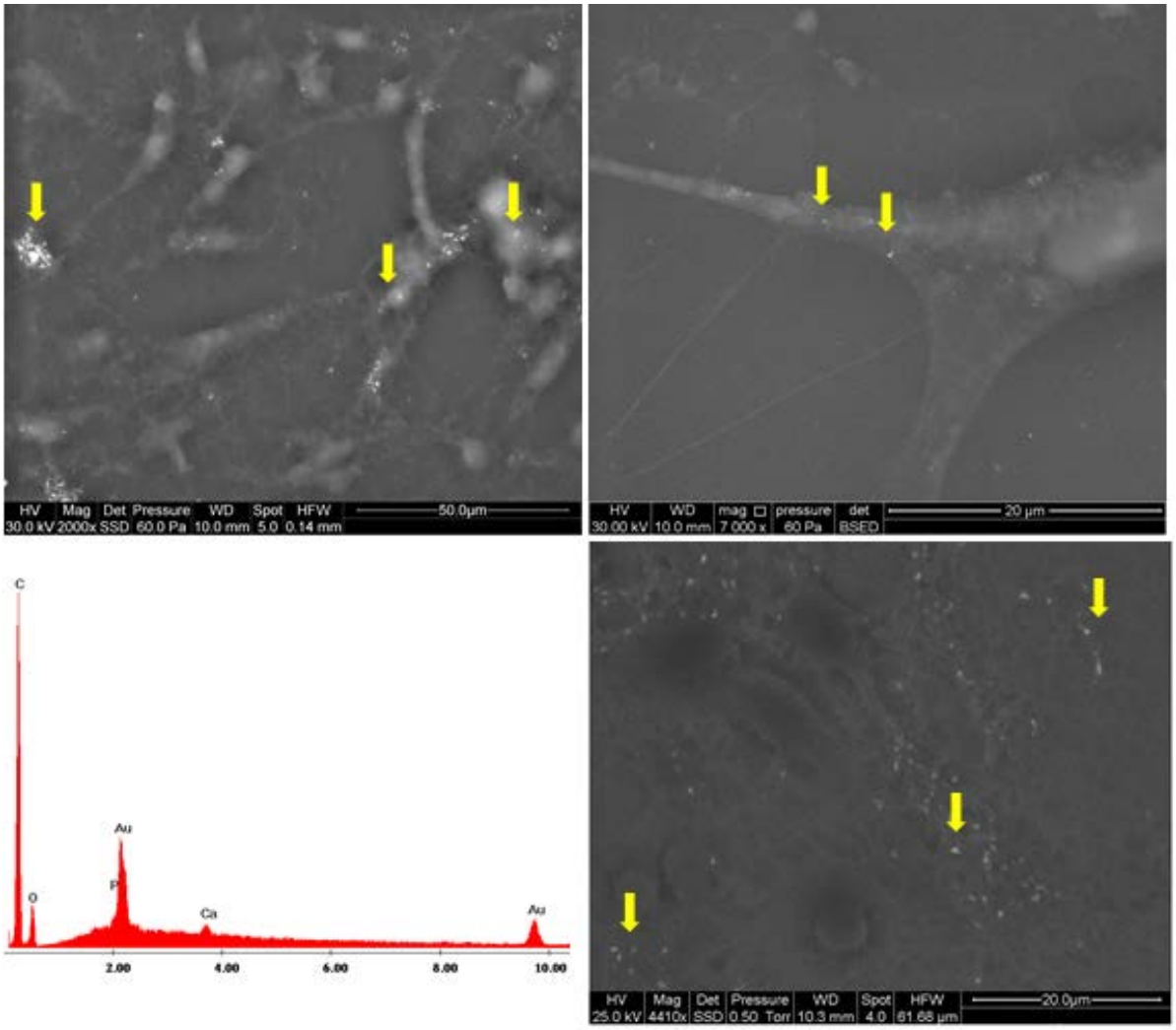

Fig.36 ESEM images at different magnifications (2000 -7000x), of primary cortical cells (neurons and glial cells) exposed to NPs of gold (arrows indicate the presence of NPs). The EDS spectrum of gold found in contact with the cells is reported in the bottom left corner image. The larger presence of NPs in astrocytes than in neurons is shown by the image at the bottom right – (4410x).

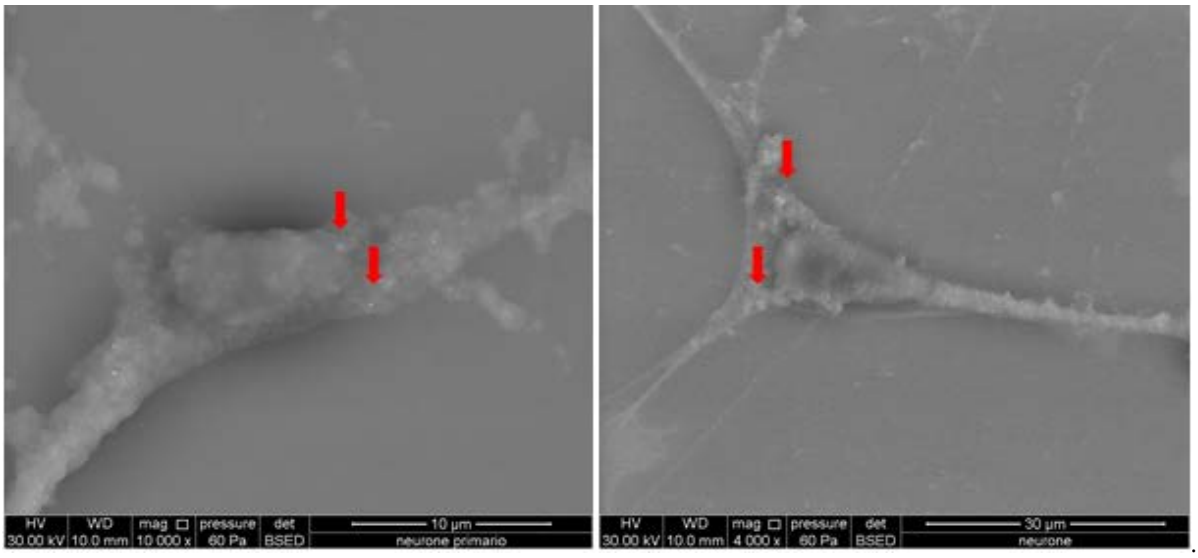

Fig.37 ESEM images at different magnifications (10.000-4000x), of primary cortical cells (neurons) exposed to NPs of iron oxide (arrows indicate the presence of NPs).

4.5 TWO-STAGE CELL TRASFORMATION ASSAY RESULTS

The two stage cell transformation was used to evaluate the NPs carcinogenicity.

The use of NPs (Au, Co, Fe_3O_4, CeO_2) as initiators or in the combination "nanoparticles + TPA", produced no tumor foci except in the case of cobalt. The presence of foci in the plates with the initiator only treatment was probably due to the use of ITES buffer which acted as a pseudo tumor promoter accelerating the cell proliferation.

Predominantly Type III foci were found after NPs treatments: Type III foci are dense, multilayered, and basophilic, with a random orientation of cells at the focus edge and invasion into the monolayer.

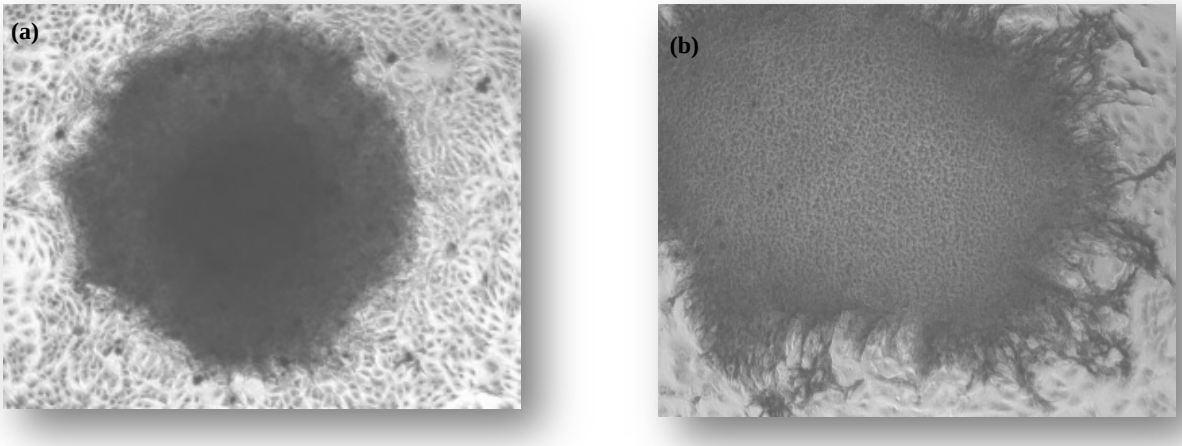

Fig. **38** Optical images of type III foci after NPs treatment. Au NPs treatment (a) and CeO_2 NPs treatment (b).

The number of foci was counted and statistically elaborated to obtain graphical data.

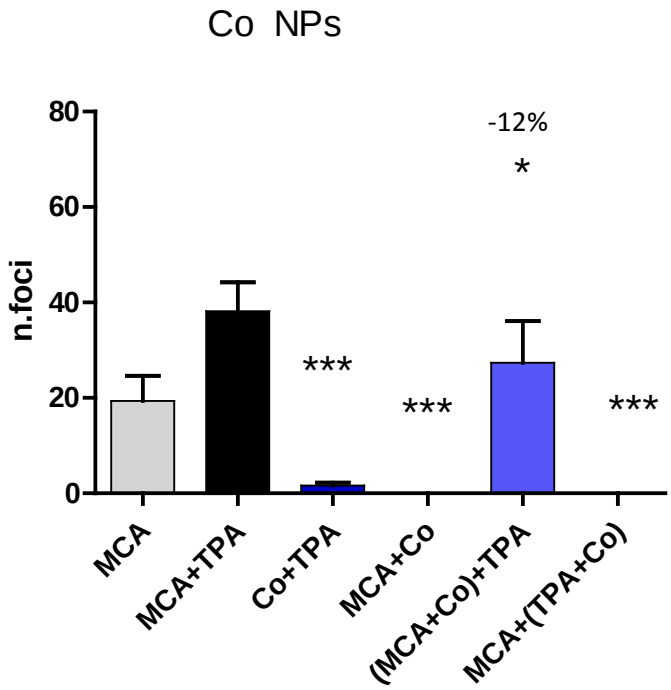

Fig. 39 Comparison between the number of foci of cancer control (MCA+TPA) compared to cells treated with various combinations of cobalt NPs. (* Significance vs MCA+TPA - *** p<0,001 vs MCA+TPA)

Cobalt NPs (Fig. 40), in spite of the toxicity found in XTT and BrdU tests, confirmed a carcinogenic effect on the 3T3 cells acting as initiators. The ability to decrease cell viability and proliferation did not prevent foci formation after only three days (72h) of exposure as Co+TPA (Fig. 39). On the contrary, using the NPs in place of the tumor promoter (TPA) as MCA+Co treatment showed an increased toxic effect due to the prolonged time of exposure (>96h). In fact, at the end of the treatment, only a few surviving cells were found upon contact. Following co-administration of cobalt particles with the initiator MCA and the treatment with the promoter TPA demonstrated the transforming effect (-12%) of the NPs despite their capability to decrease cell proliferation. In the last column, cobalt particles co-administered with the TPA promoter, showed again a strong anti-proliferative effect due to the prolonged time exposure (>96h).

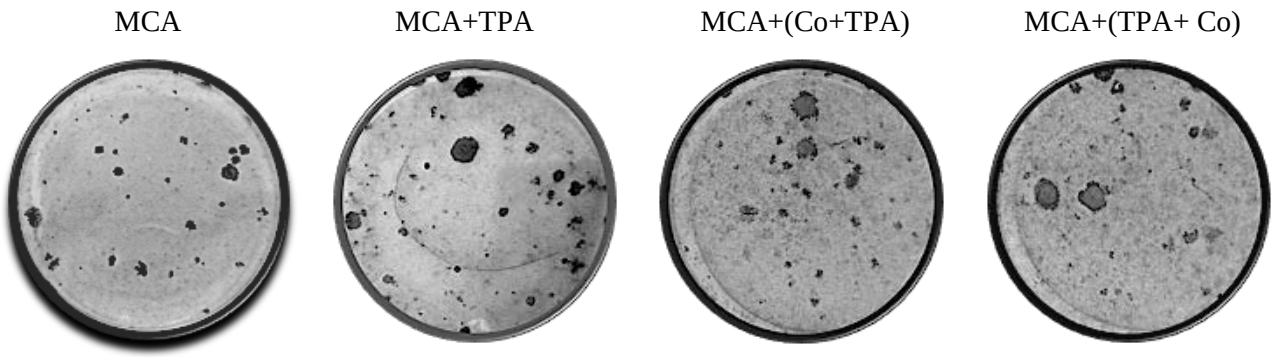

Fig. **40** Optical images of BALB 3T3 cell plates treated with MCA, TPA and the NPs in various combinations. Type III foci increased number can be clearly seen after the cobalt NPs treatment.

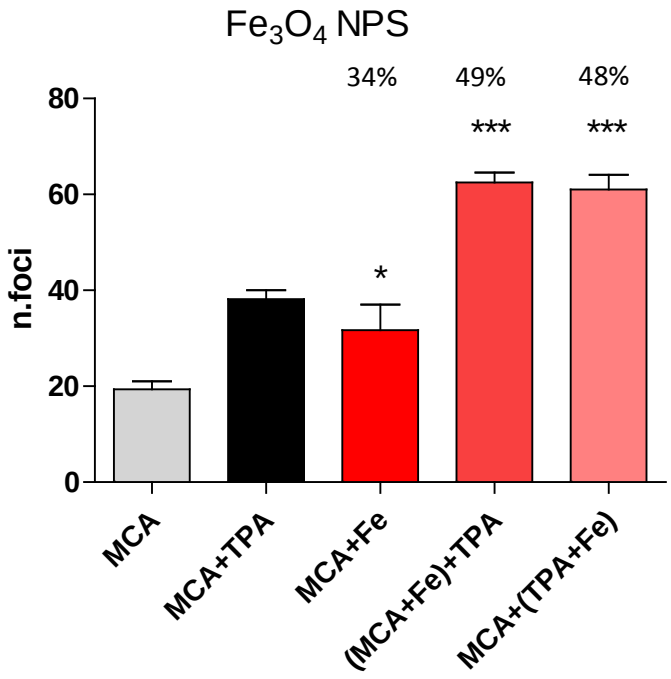

Fig. 41 Comparison between the number of foci of cancer control (MCA+TPA) compared to cells treated with various combinations of iron oxide NPs. (* Significance vs MCA+TPA - *** p<0,001 vs MCA+TPA)

Results obtained using iron oxide NPs were completely different. NPs of Fe_3O_4 administered as tumor promoters have caused a slight decrease in the number of foci in relation to its control (MCA+TPA), as shown in Figures 41 and 42. On the contrary, NPs used as co-initiators or co-promoters in association with MCA and TPA have produced a considerable increase in the number of foci, especially in cells where the NPs were used as co-initiator (49%). Iron oxide NPs were not able to generate any foci when used as initiators only.

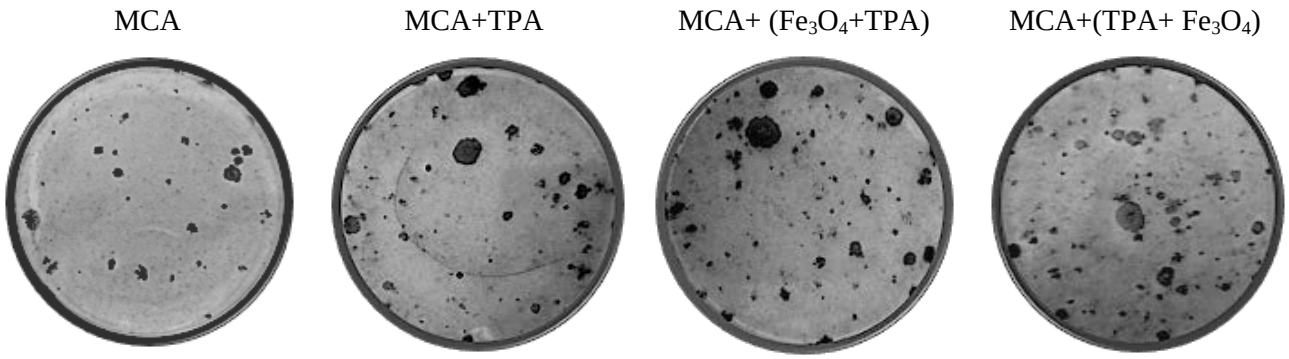

Fig. **42** Optical images of BALB 3T3 cell plates treated with MCA, TPA and the NPs in various combinations. Type III foci increased number can be clearly seen after the iron oxide NPs treatment.

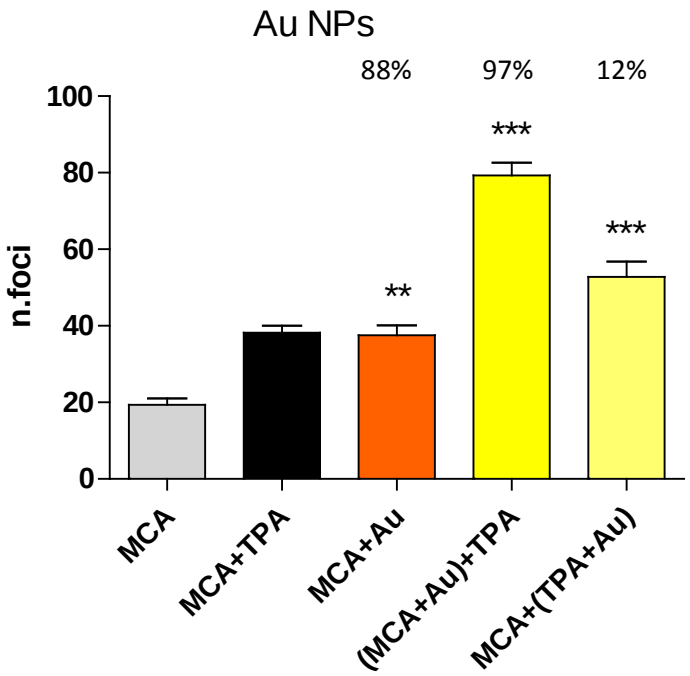

Fig. 43 Comparison between the number of foci of cancer control (MCA+TPA) compared to cells treated with various combinations of gold NPs. (* Significance vs MCA+TPA - ** p<0,001 vs MCA - *** p<0,001 vs MCA+TPA)

Similarly to iron oxide results, gold NPs were able to cause a comparable number of foci relative to the MCA+TPA control when used as promoters (Fig. 44). On the opposite, the gold NPs treatment as a function of co-tumor initiator caused an increase up to 97% in the number of foci compared to the control (Fig. 43). NPs used as co-promoters induces a slight12% increase in the number of foci.

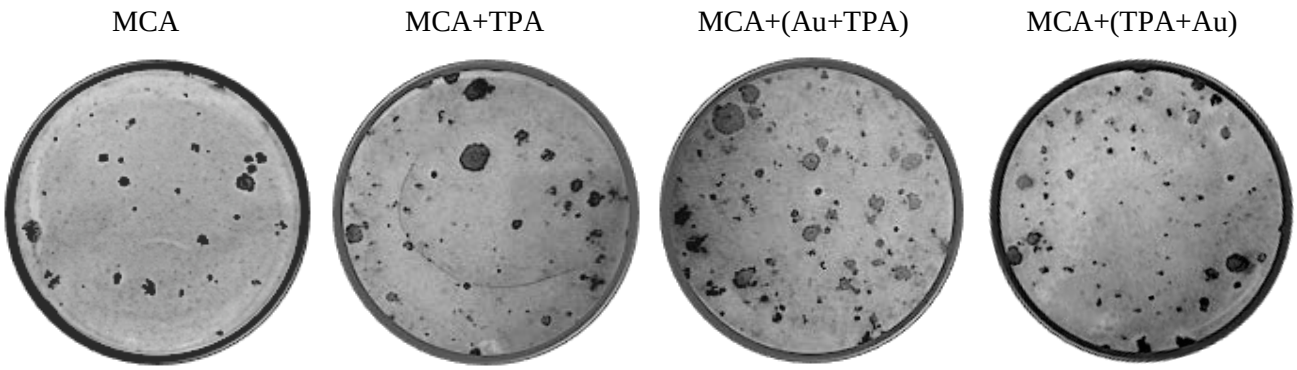

Fig. **44** Optical images of BALB 3T3 cell plates treated with MCA, TPA and the NPs in various combinations. Type III foci increased number can be clearly seen after the gold NPs treatment.

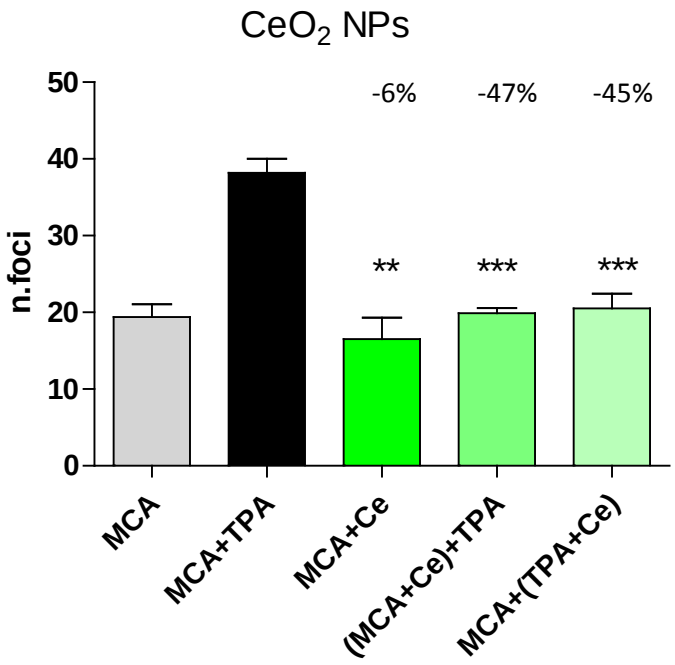

Fig. 45 Comparison between the number of foci of cancer control (MCA+TPA) compared to cells treated with various combinations of cerium oxide NPs. (** p<0,001 vs MCA - *** p<0,001 vs MCA+TPA)

On the opposite side, results obtained using cerium oxide NPs showed a general decrease in the number of foci (Fig. 46). NPs of CeO_2 administered as tumor promoters caused a slight decrease (-6%) in the number of foci in relation to its control (MCA). NPs used as co-initiators produced an evident -47% decrease in the number of foci compared to the MCA+TPA control (Fig. 45). When used as co-promoters the cerium oxide NPs were also responsible to produce a -45% decrease in the number of foci. Cerium oxide NPs were not able to generate any foci when used as initiators only.

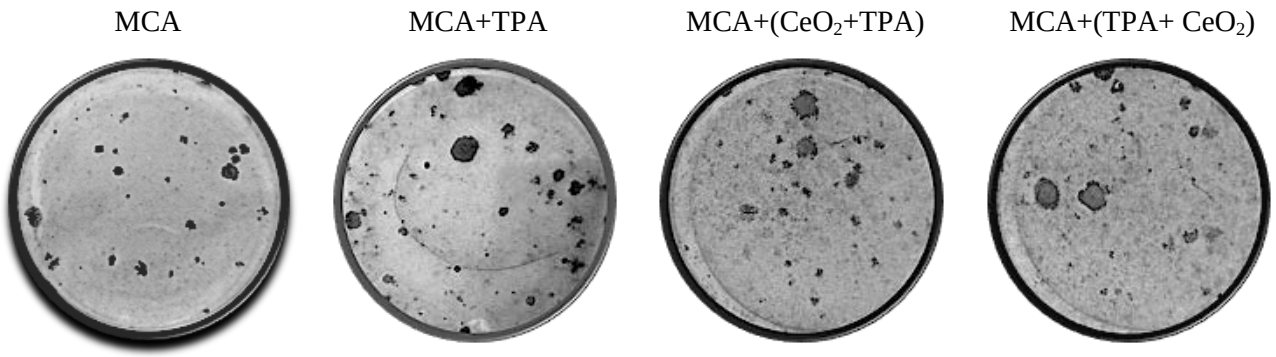

Fig. **46** Optical images of BALB 3T3 cell plates treated with MCA, TPA and the NPs in various combinations. Type III foci increased number can be clearly seen after the cerium oxide NPs treatment.

4.5.1 ESEM ANALYZES OF TYPE III FOCI

Type III foci obtained after treatments in the two-stage transformation assay were analyzed using ESEM. Type III foci appeared dense with their typical multilayered morphology: ESEM images displayed clearly cell foci invasion into the monolayer (Fig. 47). The presence of all types of NPs was found mostly coincident to cell foci although it was impossible to quantify precisely the NPs direct number.

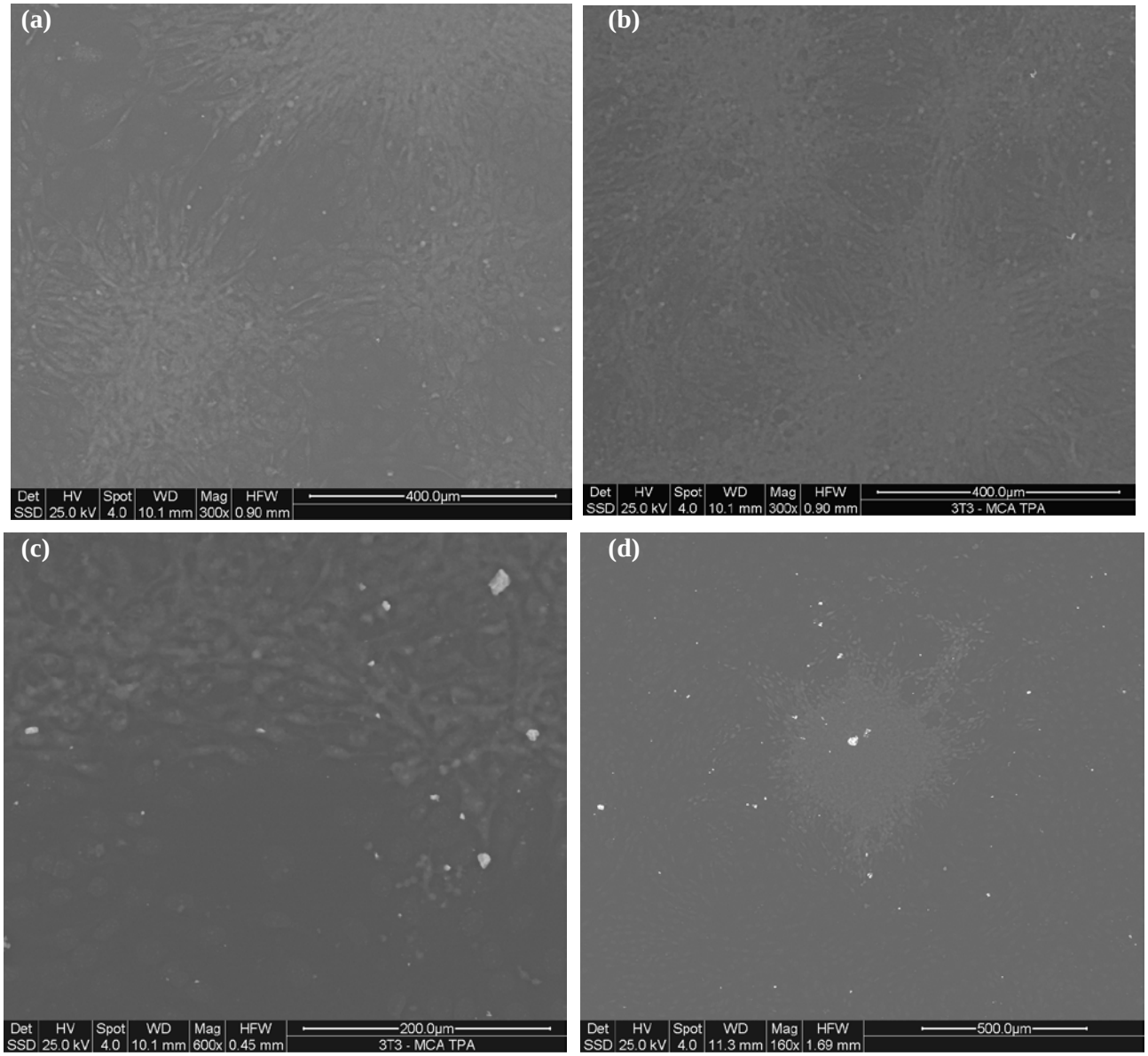

Fig.47 ESEM images at different magnifications (300-600x), of type III foci after MCA+TPA treatment (a;b), after Au-NPs treatment as co-initiator (c) and after Fe_3O_4 NPs treatment as co-initiator (d).

5. DISCUSSION

In recent years the use of metal NPs in the medical-pharmaceutical field is increased exponentially. NPs exhibit physical and chemical properties that are optimal for a wide number of biomedical applications. These applications include drug delivery, imaging techniques (AFM, MRI), cancer treatment (cancer Photothermal conversion therapy) and the detection of neurodegenerative diseases [78-83]. Gold NPs for example are now being tested in advanced imaging techniques to detect ²-amyloid inhibitors used in the treatment of Alzheimer's disease [79]. Iron oxide NPs, thanks to their paramagnetic properties, are applied to resonance imaging methods to detect the protein Tau in Alzheimer patients [82]. Iron oxide NPs are now being tested to track micro vascular alterations indicative of cerebral angiopathy due to accumulation of ²-amyloid [81]. In addition several studies have already shown that NPs of iron oxide can also reduce the aggregation of beta-amyloid in the cerebro-spinal fluids of Alzheimer patients [83].

In light of these applications it is essential to evaluate and understand the role and the toxicity of these metal particles on the human nervous system. The data obtained on rat primary neurons cultures indicate that there is no reduction in cell viability after 48/72 hours of exposure to NPs (fig. 15). However the distribution of NPs was non homogeneous, as shown in the morphological analysis (fig. 35), and their localization has involved selectively glial cells. It is clear that glial cells play a protective role towards neurons and their function may act as a shield to NPs potential toxicity. Cell viability data obtained on immortalized lines confirmed this hypothesis by showing an absence of toxicity of gold NPs on glioblastoma U-87 cells while highlighting some toxicity (16% decreased vitality at 48 hours) on neuroblastoma SHSY-5Y cells. The iron oxide NPs showed a slight toxic effect on both U-87 and SH-SY5Y cell lines at 48 hours and it last until 72h in U-87 cells. XTT toxicity data concerning cobalt and cerium oxide NPs showed a toxic effect on both neuroblastoma and glioblastoma cell lines at 48h. However this decrease was evidenced only in U-87 cells at 72h. BrdU ELISA data are comparable to XTT results: the data on gold and iron oxide NPs were very similar to XTT viability results and the only difference was found with cerium oxide NPs which did not show any significant effect on U-87 cell proliferation after 72h of treatment. These data might explain the absence of toxicity reported on rat primary cultures: in primary rat cultures ESEM analyzes showed that glial cells were able to capture nearly most of the NPs protecting neurons from NPs contact. Rat primary cultures showed no sign of morphological cell damage after NPs contact in both neuronal and glial sub-populations.

Cytotoxicity data obtained on immortalized microglia cells confirmed these data. In fact, BV-2 cells did not show any sign of toxicity after contact with all the different types of NPs at both 48 and 72h. However XTT results showed a slight alteration of cell viability with gold and iron oxide NPs at 48h which may be related to pro-inflammatory effects. ESEM analyzes showed that BV-2 cells were able to capture by phagocytosis most of the NPs. Metal NPs bio persistence inside the cells could cause long term effects not covered by relatively short (72h max) in vitro tests. Further experiments will be required on specific molecular targets to assess the NPs possible role on these cells.

The TWO-STAGE CELL TRANSFORMATION assay evaluated the ability of gold, iron oxide, cobalt and cerium oxide NPs to act as tumor initiators or tumor promoters. Gold, iron oxide and cerium oxide NPs were not capable to act as tumor initiators. In fact when these NPs were used instead of the MCA initiator no formation of foci was found. Gold and iron oxide NPs were capable to act as tumor promoters: the administration of gold or iron oxide NPs instead of the TPA promoter provided a number of foci very similar to that of the MCA + TPA control. In addition the cell exposure to gold or iron oxide NPs as co-initiators with MCA induced a much higher (>97% for Au and >49% for Fe_3O_4 NPs) number of foci than that of the MCA + TPA control. When gold and iron oxide NPs were used as co-promoters with TPA, they induced also an increase (>12% for Au and >48% for Fe_3O_4 NPs) in the number of foci compared to the MCA + TPA control. These data need a considerable attention due to their support by the very similar in vivo results obtained using iron oxide NPs and benzopyrene in Sprague-Dawley rats [93-94].

On the opposite side cerium oxide NPs results showed a totally different tendency. Cerium oxide NPs were not capable to induce any foci formation as already gold and iron oxide NPs showed. However cerium oxide NPs used instead of the TPA promoter showed a decreased (-6%) number of foci in comparison to the MCA+ TPA control. When used as co-initiators or co-promoters cerium oxide NPs decreased the number of foci respectively of -47% and -45%. Considering the XTT and BrdU ELISA data obtained on immortalized cell lines, the mechanism by which cerium oxide NPs were capable to diminish the number of foci may be related to their cytotoxicity, but still remains to be explained. In the case of cobalt NPs the two-stage transformation assays identified the NPs as initiators highlighting their ability to produce foci when used instead of the MCA initiator.

The well known cytotoxicity of cobalt NPs declined so drastically the cellular number to prevent the formation of foci when NPs were used instead of TPA promoter. Cobalt NPs administered with MCA and later treated with TPA suggested their effect as initiators, being the number of foci noted similar to MCA+ TPA control despite their toxicity. The long term of exposure of cobalt NPs administered along with the TPA promoter (>72h) did not allow to obtain, due to the high toxicity, a sufficient number of cells in plates. Cytotoxicity of cobalt has nonetheless shown his role as tumor initiator and its transforming capacity as already reported in literature [86-87].

Considering the TWO-STAGE CELL TRANSFORMATION assay data obtained on the metal NPs analyzed some hypotheses may be formulated.

The first hypothesis is that the NPs interact with the MCA initiator or TPA promoter by surface coating. These MCA/TPA coated NPs can be captured by the cells and their interaction or internalization might expose the cells to an higher dose of the tumor initiator or promoter. In fact ESEM microscopy images showed that a large number of NPs as singlet or as agglomerates were present coinciding with the presence of cancer foci. The second hypothesis involves a mechanism of long term bio persistence of the NPs. It is plausible that, each different type of NPs acts on specific cell targets with unique effects depending on the NPs physical and chemical properties. The physical prolonged presence inside the cells of the NPs might act as a persistent stimuli capable to activate or inhibit totally different molecular pathways. In this regard,

further studies are needed to evaluate NPs possible ROS production, pro-inflammatory effect and their ability to interact with proteins or DNA.

6. CONCLUSIONS

Metal NPs interaction and internalization was found significantly higher in glial (U-87, rat primary cells) and microglia (BV-2) cells than in neuronal cells (SHSY-5Y, rat primary cells). Rat primary cell line did not show any sign of citotoxicity even after massive internalization of NPs by glial cells. In vitro carcinogenic data on metal NPs showed that gold and iron oxide NPs act as co-initiators and co-promoters enhancing foci formation up to 92%. However, all the NPs tested except cobalt did not show any initiator effect. Cerium oxide NPs have shown the capability to reduce foci formation decreasing the promoter activity. The metallic NPs data obtained represent a new toxicological level of challenge, requiring advanced studies to evaluate NPs short and long term effect at neuronal level. Their involvement in the development of neurodegenerative diseases such as Alzheimer's and Parkinson's disease remains still to be tested but these preliminary studies already showed the complexity and the potential adverse effects of these new materials.

REFERENCES

1) Martinez-Finley EJ, Avila DS, Chakraborty S, Aschner M, ***"Insights from Caenorhabditis elegans on the role of metals in neurodegenerative diseases"***, *Metallomics*, 3(3): 271–279, (2011).
2) ASTM E 2456-06, ***"Terminology for Nanotechnology"***, ASTM International (2006).
3) Buzea C, Pacheco I, Robbie K, ***"Nanomaterials and nanoparticles: sources and toxicity"***, *Biointerphases*. 2:4, (2007).
4) Aitken R.J., Creerly K.S., Tran C.L.,***"Nanoparticles: an occupational hygiene review"***, *Research Report 274, Health and Safety Executive (HSE),UK*, pp.113, (2004).
5) Ostiguy C, Lapointe G, Menard L, Cloutier Y, Trottier M, Boutin M, Antoun M, Normans C, ***"Nanoparticles : actual knowledge about occupational health and safety risks and prevention measures"*** *IRSST, report- 470,* (2006).
6) Maynard AD, Aikten RJ, ***"Assessing exposure to airborne nanomaterials: current abilities and future requirements"***, *Nanotoxicology* 1: 26-41 (2007).
7) Buseck PR, Posfai M, ***"Airborne minerals and related aerosol particles: effects on climate and the environment",*** *Proc. Nat. Acad. Sci. USA* 96: 3372, (1999).
8) Sapkota A, Symons J.M, Kleissl J, Wang L, Parlange M B, Ondov J, Breysse P N, Diette GB, Eggleston PA, Buckley TJ, ***"Impact of the 2002 Canadian forest fires on particulate matter air quality in Baltimore city",*** *Environ. Sci. Technol.* 39 24 –32, (2005).
9) Taylor DA, ***"Dust in the wind"***, *Environ, Health Perspect* (2002).
10) Kittelson DB. ***"Recent measurements of nanoparticle emission from engines: Current Research on Diesel Exhaust Particles",*** *Japan Association of Aerosol Science and Technology*, Tokyo, (2001).
11) Houghton J, ***"Global warming"***, *Rep. Prog. Phys*. 68: 1343, (2005)
12) Rogers F, Arnout P, Zielinska B, Sagebiel, KE, Wagner D, Lighty JS, Sarofim AF, ***"Real-time measurements of jet aircraft engine exhaust"***, *J. Air Waste Manage Assoc.* 55:583, (2005).
13) Scames WS, Fernandez A, Wendt JO, ***"A study of fine particulate emissions from combustion of treated pulverized municipal sewage sludge"***, *Environ. Sci. Technol.* 36: 2772, (2002).
14) Lewinski N, Colvin V, Drezek R, ***"Cytotoxicity of nanoparticles"***, *Small.,* 4(1):26-49 (2008).

15) Ponti J, Colognato R, Rauscher H, Gioria S, Broggi F, Franchini F, Pascual C, Giudetti G, Rossi F, ***"Colony Forming Efficiency and microscopy analysis of multi-wall carbon nanotubes cell interaction"***, *Toxicol Lett.* 1;197(1):29-37, (2010).

16) Liu BR, Huang YW, Chiang HJ, Lee HJ, "***Cell-penetrating peptide-functionized quantum dots for intracellular delivery"***, *J. Nanosci. Nanotechnol.,* 10: 7897-905 (2010).

17) Nisman R, Dellaire G, Ren Y, Li R, Bazett-Jones DP, ***"Application of quantum dots as probes for correlative fluorescence, conventional, and energy-filtered transmission electron microscopy"***, *J Histochem Cytochem.,* 52(1):13-8 (2004).

18) *Wang X, Yang L, Chen Z, Dong M*, ***"Application of nanotechnology in cancer therapy and imaging"***, *CA Cancer J Clin.,* 58:97–110 (2008).

19) Cheng J, Teply BA, Sherifi I, Sung J, Luther G, Gu FX, Levy-Nissenbaum E, Radovic-Moreno AF, Langer R, Farokhzad OC, ***"Formulation of functionalized PLGA-PEG nanoparticles for in vivo targeted drug delivery"***, *Biomaterials.,* 28(5):869-76, (2007).

20) Moore A, Weissleder R, Bogdanov A, ***"Uptake of dextran-coated monocrystalline iron oxides in tumor cells and macrophages"***, *J. Magn Reson Imaging*, 7:1140–1145 (1997).

21) Namiki Y, Fuchigami T, Tada N, Kawamura R, Matsunuma S, Kitamoto Y, Nakagawa M, "***Nanomedicine for cancer: lipid-based nanostructures for drug delivery and monitoring"***, *Acc Chem Res.,* 18;44(10):1080-93, (2011).

22) Oberdörster G, Oberdörster E, Oberdörster J, ***"Nanotoxicology: an emerging discipline evolving from studies of ultrafine particles"***, *Environ Health Perspect.,* 113(7):823-39. (2005).

23) Hussain N, Jaitley V, Florence AT, ***"Recent advances in the understanding of uptake of microparticulate across the gastrointestinal lymphatics ",*** *Adv. Drug Delivery Rev*. 50 107-142 (2001).

24) Ballestri M, Baraldi A, Gatti AM, Furci L, Bagni A, Loria P, Rapanà RM, Carulli N, Albertazzi A, ***"Liver and kidney foreign bodies granulomatosis in a patient with malocclusion, bruxism, and worn dental prostheses"***, *Gastroenterology,* 121(5):1234-8. (2001).

25) Gatti AM, ***"Biocompatibility of micro- and nano-particles in the colon",*** *Biomaterials* 385-392 (2004).

26) Semmler M, Seitz J, Erbe F, Mayer P, Heyder J, Oberdörster G et al., ***"Long-term clearance kinetics of inhaled ultrafin einsoluble iridium particles from the rat lung, including tran-sient translocation into secondary organs",*** *Inhal Toxicol.,* 16:453-459 (2004).

27) Donaldson K, Tran L, Jimenez L, Duffin R, Newby DE, Mills N et al., ***"Combustion-derived nanoparticles: a review of their toxicology following inhalation exposure"***, Fibre Toxicol, 2:10 (2005).

28) Ferin J, Oberdörster G, ***"Translocation of particles from pulmonary alveoli into the interstitium"***, *J. Aerosol Med.*, 5:179–187 (1992).

29) Geiser M, Rothen-Rutishauser B, Kapp N, Schürch S, Kreyling W, Schulz H, et al., ***"Ultrafine particles cross cellular membranes by nonphagocytic mechanisms in lungs and in cultured cells.",*** *Environ. Health Perspect*, 113: 1555-60 (2005).

30) Vogt A, Combadiere B, Hadam S, Stieler KM, Lademann J, Schaefer H, Autran B, Sterry W, Blume-Peytavi U, ***"40 nm, but not 750 or 1,500 nm, nanoparticles enter epidermal CD1aþ cells after transcutaneous application on human skin"***, *J. Invest. Dermatol.*, 126:1316–22, (2006).

31) Nohynek GJ, Lademann J, Ribaud C, Roberts MS, ***"Grey goo on the skin? Nanotechnology, cosmetic and sunscreen safety"***, *Crit. Rev. Toxicol.* 37 251-277, (2007).

32) Serpone N, Salinaro A, Emeline A, ***"Deleterious effects of sunscreen titanium dioxide nanoparticles on DNA: efforts to limit DNA damage by particle surface modification"***, *Proc. SPIE*, 4258 86-98, (2001).

33) Reddy ST, Van der Vlies AJ, Simeoni E, Angeli V, Randolph GJ, O'Neil CP, Lee K, Swartz MA, Hubbell JA, ***"Exploiting lymphatic transport and complement activation in nanoparticle vaccines"***, *Nat Biotechnol.*, 25(10):1159-64, (2007)

34) Ravizzini G, Turkbey B, Barrett T, Kobayashi H, Choyke PL, ***"Nanoparticles in sentinel lymph node mapping",*** *Wiley Interdiscip Rev Nanomed Nanobiotechnol.*, 1(6):610-23, (2009).

35) Semmler-Behnke M, Kreyling WG, Lipka J, Fertsch S, Wenk A, Takenaka S, Schmid G, Brandau W, ***"Biodistribution of 1.4- and 18-nm gold particles in rats"***, *Small.*, 4, 2108–2111, (2008).

36) Geiser M, Casaulta M, Kupferschmid B, Schulz H, Semmler-Behnke M, Kreyling W, ***"The role of macrophages in the clearance of inhaled ultrafine titanium dioxide particles"***, *Am. J. Respir. Cell Mol. Biol.* 38, 371–376, (2008).

37) Nemmar A, Hoylaerts MF, Hoet PH, Dinsdale D, Smith T, Xu H, Vermylen J, Nemery B, ***"Ultrafine particles affect experimental thrombosis in an in vivo hamster model"***, *Am. J. Respir. Crit. Care Med.* 166, 998–1004 (2002).

38) Gatti AM, Montanari S, Monari E, Gambarelli A, Capitani F, Parisini B, ***"Detection of micro- and nano-sized biocompatible particles in the blood"***, *J. Mater. Sci. Mater. Med*., 15 469-472, (2005).

39) Pope CA, Burnett RT, Thurston GD, Thun MJ, Calle EE et al. ***"cardiovascular mortality and long-term exposure to particulate air pollution epidemiological evidence of general pathophysiological pathways of disease"***, *Circulation*, 109:71-77, (2004).

40) Kusaka Y, Yokoyama K, Sera Y, Yamamoto S, Sone S, Kyono H, Shirakawa T, Goto S, ***"Respiratory diseases in hard metal workers: an occupational hygiene study in a factory"***, *Br. J. Ind. Med.*, 43: 474-85, (1986).

41) Inoue K, Takano H, ***"Aggravating impact of nanoparticles on immune-mediated pulmonary inflammation"***, *Scientific World Journal*, 11: 382-90, (2011).

42) Xia T, Kovochich M, Brant J, Hotze M, Sempf J, Oberley T, Sioutas C, Yeh JI, Wiesner MR, Nel AE, ***"Comparison of the abilities of ambient and manufactured nanoparticles to induce cellular toxicity according to an oxidative stress paradigm",*** *Nano Lett.* 6 1794-1807, (2006).

43) Li N, Sioutas C, Cho A, Schmitz D, Misra C, Sempf J et al., ***"Ultrafine particulate pollutants induce oxidative stress and mitochondrial damage"***, *Environ Health Perspect.* 111(4):455-60, (2003).

44) Boverhof DR, David RM, ***"Nanomaterial characterization: considerations and needs for hazard assessment and safety evaluation"***, *Anal Bioanal Chem.* 396(3):953-61, (2010).

45) Xiaoyan L, Yu T, Qinqin Z, Tingting J, Shun X and Xiaohui F, ***"Integrated metabonomics analysis of the size-response relationship of silica nanoparticles-induced toxicity in mice"***. *Nanotechnology*, 4;22(5):055101, (2011).

46) Oberdörster G, Sharp Z, Atudorei V, Elder A, Gelein R, Lunts A ***"Extrapulmonary translocation of ultrafine carbon particles following whole-body inhalation exposure of rats".*** *J. Toxicol. Environ. Health*, A65 1531-1543, (2002).

47) Brown DM, Donaldson K, Borm PJ, Schins RP, Dehnhardt M, Gilmour P, Jimenez LA, Stone V, ***"Calcium and ROS-mediated activation of transcription factors and TNF cytokine gene expression in macrophages exposed to ultrafine particles"***, *Lung Cell. Mol. Physiol.* 286 L344-L353, (2004).

48) Long H, Shi T, Borm P J, Määttä J, Husgafvel-Pursiainen K, Savolainen K, Krombach F, ***"ROS mediated TNF alfa and MIP-2 gene expression in alveolar macrophages exposed to pine dust"***, *Part. FibreToxicol.* 1:3, (2004).

49) Lim Y, Kim S H, Cho Y J, Kim K A, Oh M W, Lee K H ***"Silica-induced oxygen radical generation in alveolar macrophages",*** *Ind. Health*, 35 380-387 (1997).

50) Ferreira PC, Piai KA, Takayanagui AMM, Segura-Muñoz SI, *"**Aluminum as a risk factor for Alzheimer's disease"**, Rev Latino-am Enfermagem*, 16(1):151-7, (2008).

51) Martyn CN, Coggan D, Inskip H, Lacey RF, Young WF, ***"Aluminum concentrations in drinking water and risk of Alzheimer's Disease"***, *Epidemiology*, 8(3):281-6, (1997).

52) Rondeau V, Jacqmin-Gadda H, Commenges D, Helmer C, Dartigues JF, ***"Aluminum and silica in drinking water and the risk of Alzheimer's Disease or cognitive decline: findings from 15-year follow-up of the PAQUID cohort"***, *American Journal of Epidemiology*, Vol. 169, No. 4 (2008).

53) Bharathi P, Vasudevaraju M, Govindaraju AP, Palanisamy K, Sambamurti KSJ, ***"Molecular toxicity of aluminum in relation to neurodegeneration"***, *Indian J Med Res* 128, 545-556, (2008).

54) Peters A, Veronesi B, Calderón-Garcidueñas L, Gehr P, Chen LC, Geiser M, Reed W, Rothen-Rutishauser B, Schürch S, Schulz H, ***"Translocation and potential neurological effects of fine and ultrafine particles a critical update"***, *Part. Fibre Toxicol.*, 3:13, (2006).

55) Oberdorster G, Sharp Z, Atudorei V, Elder A, Gelein R, Kreyling W, Cox C, ***"Translocation of inhaled ultrafine particles to the brain"***, *Inhal. Toxicol.*, 16:437-45, (2004).

56) Elder A, Gelein R, Silva V, Feikert T, Opanashuk L, Carter J, Potter R, Maynard A, Ito Y, Finkelstein J et al, ***"Translocation of inhaled ultrafine manganese oxide particles to the central nervous system",*** *Environ Health Perspect*, 114:1172-8, (2006).

57) Oberdörster G, Sharp Z, Atudorei V, Elder A, Gelein R, Lunts A, ***"Extrapulmonary translocation of ultrafine carbon particles following whole-body inhalation exposure of rats"***, *J. Toxicol. Environ. Health A* 65 1531-1543, (2002).

58) Block ML, Calderón-Garcidueñas L, ***"Air pollution: mechanisms of neuroinflammation and CNS disease"***, *Trends. Neurosci.*, 32: 506-16, (2009).

59) Borm PJA, Robbins D, Haubold S, Kuhlbusch T, Fissan H, Donaldson K, Schins RPF, Stone V, Kreyling W, Lademann J, Krutmann J, Warheit D, Oberdorster E, ***"The potential risks of nanomaterials: a review carried out for ECETOC"*** (*review) Part. Fibre Toxicol*. 3 11, (2006).

60) Lockman PR, Koziara JM, Mumper RJ, Allen DD, ***"Nanoparticle surface charges alter blood brain barrier integrity and permeability",*** *J. Drug Targeting* 12 635-641, (2004).

61) Wang J, Liu Y, Jiao F, Lao F., Li W., Gu Y., Li Y., Ge C., Zhou G., Li B., Zhao Y, Chai Z, Chen C, ***"Time-dependent translocation and potential impairment on central nervous system by intranasally instilled TiO(2)nanoparticles"***, *Toxicology*, 254: 82-90, (2008).

62) Shin JA, Lee EJ, Seo SM, Kim HS, Kang JL, Park EM, ***"Nanosized titanium dioxide enhanced inflammatory responses in the septic brain of mouse"***, *Neuroscience*, 165: 445-54, (2010).

63) Antonini JM, Sriram K, Benkovic SA, Roberts JR, Stone S, Chen BT, Schwegler-Berry D, Jefferson AM, Billig BK, Felton CM, Hammer MA, Ma F, Frazer DG, O'Callaghan JP, Miller DB, ***"Mild steel welding fume causes manganese accumulation and subtle neuroinflammatory changes but not overt neuronal damage in discrete brain regions of rats after short-term inhalation exposure"***, *Neurotoxicology*, 30: 915-25, (2009).

64) Yu LE, Lanry Yung L-Y, Ong C-N, Tan Y-L, Suresh Balasubramaniam K, Hartono D, Shui G, Wenk MR, Ong W-Y: ***"Translocation and effects of gold nanoparticles after inhalation exposure in rats"***, *Nanotoxicology*, 1:235-242 (2007).

65) Sarkozi L, Horvath E, Konya Z, Kiricsi I, Szalay B, Vezer T, Papp A, ***"Subacute intratracheal exposure of rats to manganese nanoparticles: behavioral, electrophysiological, and general toxicological effects"***. *Inhal Toxicol*, 21:83-91 (2009).

66) Dopp E, Yadav S, Ansari FA, Bhattacharya K, von Recklinghausen U, Rauen U, Rodelsperger K, Geh S, Rahman Q, ***"ROS-mediated genotoxicity of asbestos-cement in mammalian lung cells in vitro".*** *Part. Fibre Toxicol* 2: 9, (2005).

67) Wu J, Sun J, ***"Investigation on mechanism of growth arrest induced by iron oxide nanoparticles in PC12 cells".*** *J Nanosci Nanotechnol*. 11(12):11079-83, (2011).

68) Perreault F, Pedroso Melegari S, Henning da Costa C, de Oliveira Franco Rossetto AL, Popovic R, Gerson Matias W, ***"Genotoxic effects of copper oxide nanoparticles in Neuro 2A cell cultures".*** *Sci Total Environ*. 15;441:117-24, (2012)

69) Gremo F, Sogos V, Ennas MG, Meloni A, Persichini T, Colasanti M, Lauro GM, ***"Features and functions of human microglia cells".*** *Adv Exp Med Biol.* 429:79-97, (1997).

70) Iadecola C, Li J, Ebner TJ, Xu X, ***"Nitric oxide contributes to functional hyperemia in cerebellar cortex.*** *Am J Physiol.* 268(5 Pt 2):R1153-62, (1995).

71) Paresce DM, Chung H, Maxfield FR, ***"Slow degradation of aggregates of the Alzheimer's disease amyloid beta-protein by microglial cells".*** *J Biol Chem.*,14;272(46):29390-7, (1997)

72) Ryu JK, Shin WH, Kim J, Joe EH, Lee YB, Cho KG, Oh YJ, Kim SU, Jin BK, ***"Trisialoganglioside GT1b induces in vivo degeneration of nigral dopaminergic neurons: role of microglia".*** *Glia.*, 1;38(1):15-23 (2002).

73) Combs CK, Karlo JC, Kao SC, Landreth GE, ***"beta-Amyloid stimulation of microglia and monocytes results in TNFalpha-dependent expression of inducible nitric oxide synthase and neuronal apoptosis".*** *J Neurosci.* 15;21(4):1179-88 (2001).

74) Long TC, Tajuba J, Sama P, Saleh N, Swartz C, Parker J, Hester S, Lowry GV, Veronesi B, ***"Nanosize titanium dioxide stimulates reactive oxygen species in brain microglia and damages neurons in vitro".*** *Environ Health Perspect.* 115(11):1631-7 , (2007).

75) Long TC, Saleh N, Tilton RD, Lowry GV, Veronesi B, ***"Titanium dioxide (P25) produces reactive oxygen species in immortalized brain microglia (BV2): implications for nanoparticle neurotoxicity".*** *Environ Sci Technol.* 15;40(14):4346-52, (2006).

76) Wang Y, Wang B, Zhu MT, Li M, Wang HJ, Wang M, Ouyang H, Chai ZF, Feng WY, Zhao YL, ***"Microglial activation, recruitment and phagocytosis as linked phenomena in ferric oxide nanoparticle exposure".*** *Toxicol Lett.* 10;205(1):26-37, (2011).

77) Choi J, Zheng Q, Katz HE, Guilarte TR, ***"Silica-based nanoparticle uptake and cellular response by primary microglia".*** *Environ Health Perspect.*, 118(5): 589–595, (2010).

78) Boisselier E., Astruc D, ***"Gold nanoparticles in nanomedicine: preparations, imaging, diagnostics, therapies and toxicity",*** *Chem. Soc. Rev.*, 38 1759-1782 (2009).

79) Geng J, Qu K, Ren J, Qu X, ***"Rapid and efficient screening of Alzheimer's disease ²-amyloid inhibitors using label-free gold nanoparticles",*** *Mol Biosyst.*, 6(12):2389-91, (2010).

80) Kim JE, Shin JY, Cho MH, ***"Magnetic nanoparticles: an update of application for drug delivery and possible toxic effects",*** *Arch Toxicol.*, 86(5):685-700, (2012).

81) Beckmann N, Gérard C, Abramowski D, Cannet C, Staufenbiel M, ***"Noninvasive magnetic resonance imaging detection of cerebral amyloid angiopathy-related microvascular alterations using superparamagnetic iron oxide particles in APP transgenic mouse models of Alzheimer's disease: application to passive Abeta immunotherapy",*** *J. Neurosci.*, 31(3): 1023-31, (2011).

82) Lee JH, Huh YM, Jun YW, Seo JW, Jang JT, Song HT, Kim S, Cho EJ, Yoon HG, Suh JS, Cheon J, ***"Artificially engineered magnetic nanoparticles for ultrasensitive molecular imaging",*** *Nat. Med.*, 13(1):95–99, (2007).

83) Ga~ová Z, Antoaová A, Kriatofiková Z, Bartoa A, Rí•ný J, Cechová L, Klaschka J, Rípová D, ***"Attenuated antiaggregation effects of magnetite nanoparticles in cerebrospinal fluid of people with Alzheimer's disease",*** *Mol Biosyst.*, 6(11):2200-5, (2010).

84) Horev-Azaria L, Kirkpatrick CJ, Korenstein Ret, Marche PN, Maimon O, Ponti J, Romano R, Rossi F, Golla-Schindler U, Sommer D, Uboldi C, Unger RE, Villiers C., ***"Predictive***

toxicology of cobalt nanoparticles and ions: comparative in vitro study of different cellular models using methods of knowledge discovery from data", *Toxicol Sci*,122(2):489-501, (2011).

85) Papis E, Rossi F, Raspanti M, Dalle-Donne I, Colombo G, Milzani A, Bernardini G, Gornati R, ***"Engineered cobalt oxide nanoparticles readily enter cells"***, *Toxicol Lett.*, 28;189(3):253-9, (2009).

86) Ponti J, Sabbioni E, Munaro B, Broggi F, Marmorato P, Franchini F, Colognato R, Rossi F. ***"Genotoxicity and morphological transformation induced by cobalt nanoparticles and cobalt chloride: an in vitro study in Balb/3T3 mouse fibroblasts",*** *Mutagenesis.*, 24(5):439-45, (2009).

87) De Boeck M, Kirsch-Volders M, Lison D, ***"Cobalt and antimony: genotoxicity and carcinogenicity"***. *Mutat Res.*, 533(1-2):135-52, (2003).

88) Lee TL, Raitano JM, Rennert OM, Chan SW, Chan WY***, "Accessing the genomic effects of naked nanoceria in murine neuronal cells",*** *Nanomedicine*, 8(5):599-608, (2012).

89) Nalabotu SK,Kolli MB, Triest WE, Ma JY, Manne ND, Katta A, Addagarla HS, Rice KM, Blough ER, ***"Intratracheal instillation of cerium oxide nanoparticles induces hepatic toxicity in male Sprague-Dawley rats",*** *Int J Nanomedicine*, 6:2327-35, (2011).

90) Kuroki T, Sasaki K, ***"Relationship between in-vitro cell transformation and in-vivo carcinogenesis based on available data on the effects of chemicals"***, IARC Sci Publ.; 67:93-118 (1985).

91) Sakai A, Fujiki H, ***"Promotion of BALB/3T3 cell transformation by the okadaic acid class of tumor promoters, okadaic acid and dinophysistoxin-1"***, Jpn J Cancer Res. May;82(5):518-23.(1991).

92) Kajiwara Y, Ajimi S, Hosokawa A, Maekawa K, ***"Improvement of carcinogen detection in the BALB/3T3 cell transformation assay by using a rich basal medium supplemented with low concentration of serum and some growth factors",*** Mutat Res. Sep 18;393(1-2):81-90 (1997).

93) Gosset P, Shirali P, Marez T, Boutin AC, Balduyck M, Huet G, Venembre P, Haguenoer JM, ***"Toxicity of ferric oxide and benzo[a]pyrene alone or in combination in respiratory tract of Sprague Dawley rats",*** *Cent Eur J Public Health.*, 4 Suppl:56-7, (1996).

94) Garry S, Nesslany F, Aliouat E, Haguenoer JM, Marzin D, ***"Hematite (Fe_2O_3)) enhances benzo[a]pyrene genotoxicity in endotracheally treated rat, as determined by Comet Assay".*** *Mutat Res.* 8;538(1-2):19-29, (2003).

ACKNOWLEDGEMENTS

First of all I would like to thank my supervisor, Prof. Fabio Tascedda, for his support and kindness. He gave me the chance to follow my own path and to continue my studies.

This research was related to the past European Community project called DIPNA "Development of an Integrated Platform for Nanoparticle Analysis to verify their possibly toxicity and the eco-toxicity" (FP6-NMP 2006-STRP 031231). Thanks to Prof. F. Tascedda many unsolved trials were finally resolved.

I am so grateful to my co-tutor and friend Prof. Lorenzo Corsi, for his excellent guidance and advice during my entire research activity. I sincerely appreciated to have such a supportive co-tutor. I enjoyed his interest in my research as well as the fruitful discussions. I became deeply passionate in my studies thanks to his dedication and knowledge. I will always truly see him as a guide and a brilliant scientist.

Special thanks must be addressed to all the other personnel of the University of Modena and Reggio Emilia with whom I shared my lab work: Dr. Miriam Hanuskova, Dr. Roberta Salvatori, Dr. Jonathan Vinet and Dr. Franco Farina.

Further thanks go to Dr. Mauro Zapparoli and Dr. Cinzia Restani for their technical support about ESEM analysis and Confocal Microscopy. Next, I would also like to acknowledge the extremely important consulting and advising help given by Dr. Eudald Casals Mercadals from the University of Barcelona.

I sincerely thank Prof. Giulia Puja: she provided great help in difficult moments and showed me a tremendous kindness. Her support on most of my work was vital. I have not the words to thank her enough.

In the end and really most importantly, special thanks to my colleague and beloved Dr. Erica Artoni who shared the road everyday with me and gave me the focus and the strength to never give up. This thesis is dedicated to her, because she is the most brilliant biotechnologist I've ever know and the finding of my life.

To my father and my mother, they always deserved a better scientist than me, but to them it seems I am really enough. Thank you from the bottom of my heart.